Ben-Gurion University of the Negev
Faculty of Engineering Sciences
Department of Mechanical Engineering

Position Control of a Pneumatic Actuation System

Thesis submitted in partial fulfillment
of the requirements for the degree of
"Master of Science"

By

Eddie Zisser

February 2013

Position Control of a Pneumatic Actuation System

Thesis submitted in partial fulfillment
of the requirements for the degree of
"Master of Science"

By

Eddie Zisser

Author: _____ Date: _____

Approved by the advisors

Amir Shapiro: _____ Date: _____

Raziel Riemer: _____ Date: _____

Chairman of Graduate Studies Committee:_____ Date:_____

February 2013

To my wife, Tsivi

Acknowledgments

I would especially like to thank my advisors, Amir Shapiro and Raziel Riemer, for their help and support during the past three years. I am honored to be their student and hope to continue working with both of them. I would also like to thank Moshe Miller for his excellent work, which significantly assisted me with the experimental aspect of the thesis, Jonatan Bar Asher and Chen Baraf for their work on the electronic circuit, and Hanoch Efraim for good and handy advice on various issues concerning the test rig.

Abstract

Pneumatic actuation systems have been considered for many years as a controversial subject in the fields of automation and control. Their main advantages, such as high power to weight ratio, cleanliness, low cost, reliability, and a simple mechanism, have contributed to their widespread distribution, especially for implementation in automated production lines and industrial tools. On the other hand, the compressibility of the working media (usually air) makes it difficult to accurately anticipate their dynamic behavior. This disadvantage traditionally restricts the control development effort of open-loop applications where accurate motion is not required.

In this thesis we develop a position control of a pneumatic actuation system. By applying the nonlinear *backstepping* method, the controlled actuator demonstrates accurate trajectory tracking while being subjected to disturbances of a time varying external force. To prove the applicability of the method, we have implemented the controller on a test rig. The reported test results demonstrate excellent performance tracking sinusoidal and square wave reference signals. During the experiment, the magnitude of the disturbing external force varied between 250[N] to 1050 [N].

As a preliminary step for the control design, we propose a different approach to the modeling methodology of a pneumatic system. Instead of using the traditional force analysis, we derive the actuator's dynamic model based on energy method. First we define the kinetic energy and potential energy, combine them to formulate the Lagrangian of the actuator, then by using the Euler-Lagrange equation we derive the system's equation of motion.

Although we design the control based on a simplified mass flow-rate model, we include in the appendix an original and throughout methodology for its modeling. We utilize an experimental identification procedure in order to fit

a three dimensional model for the mass flow-rate as a function of the input to the valve and the pressure in the ports. The method, which can be applied to other types of valves, shows a very good model correlation.

Contents

List of Figures

1. Introduction

Pneumatics is a discipline that deals with the mechanical properties of gases, such as pressure and density, and applies the principles to the use of compressed gas as a source of power in solving engineering problems. The most widely used compressed gas is air, and thus its use has become synonymous with the term pneumatics [1].

1.1. Literature Review on Pneumatics

The use of air as an energy transfer medium can be traced back more than 2000 years. The *pipe organ*, for example, which originated approximately in the third century B.C. and is still in use today in churches and cathedrals, is a musical instrument that produces sound by driving pressurized air through wooden or metal pipes. A more modern application is the *pneumatic tube* (or *capsule pipeline*), illustrated in Figure 1.1[1], which was invented in 1806. It is a system in which cylindrical containers are propelled through a network of tubes by compressed air or by partial vacuum. The tubes are used for transporting solid objects, as opposed to conventional pipelines, which transport fluids. With the evolution of electric power, this form of energy transfer became rare.

[1] The original caption of the figure: The Pneumatic Passenger Railway, as Erected at the American Institute, Fourteenth Street, New-York, 1867. Taken from "The Pneumatic Dispatch" by Alfred Ely Beach, via Wikipedia.

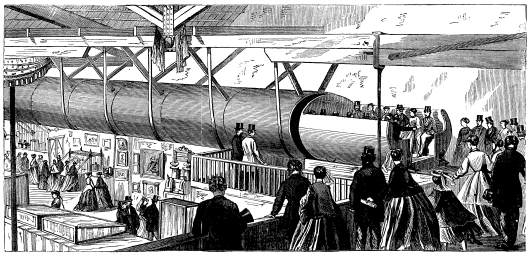

Figure 1.1.: Alfred Ely Beach's experimental pneumatic elevated subway - 1867

A very successful application of pneumatics is the air logic control system, consisting of primary logic units such as '*And*', '*Or*', '*Relay*' and more. Pneumatic logic is a reliable and functional control method for automation in industrial processes, and began in around the 1960s. In recent years these systems have largely been replaced by electrical control systems.

Today, pneumatics is mainly used in actuation systems, where pressure is converted to force and translational displacement by a piston in a circular bore. These actuators have a simple design, can be very fast, and do not overheat. The absence of heat generation allows a compact design and an excellent ratio of power to weight. In contrast to electric motion control systems, no heavy motors with complex gearing are required if the pneumatic system is used. In addition, pneumatic systems can be used with direct drive mechanisms for easy implementation of force control application [2].

1.2. Motivation and Goals

The autonomous robotics lab at the Ben-Gurion University of the Negev hosts a project of developing an autonomous quadruped robot. The robot, shown in Figure 1.2, is actuated by twelve pneumatic actuation systems that are integrated in its four legs. In order to achieve a consistent and efficient gait, each actuation system needs to be precisely controlled.

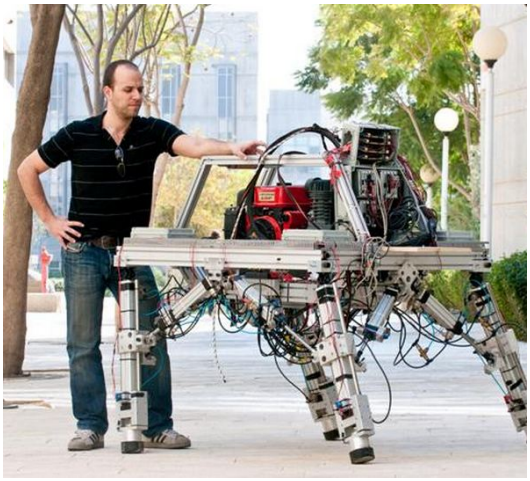

Figure 1.2.: Quadruped robot developed at the Ben-Gurion University

The major goal of this thesis is to design a motion control for the pneumatic actuators of the quadruped robot. Therefore, the controller is required to demonstrate high accuracy to allow for efficient gait. Regarding the varying load acting on the legs of the walking robot, the controller must also withstand disturbances due to a varying external force, which are a consequence of the robot's weight, inertia, and leg posture.

1.3. The Pneumatic System Under Scope

Generally, a pneumatic actuation system is composed of five basic elements: (1) the pneumatic actuator (or just actuator), which is the element that converts the pressured air into motion; (2) a control valve that either controls the pressure in different parts of the system or controls the flow into and out of the actuator; (3) sensors that close the control loop with (4) a computer, which calculate and execute the control signal to the valve. The valve is also connected to (5) a pneumatic source, which provides a steady, clean, and dry supply of air in a constant pressure.

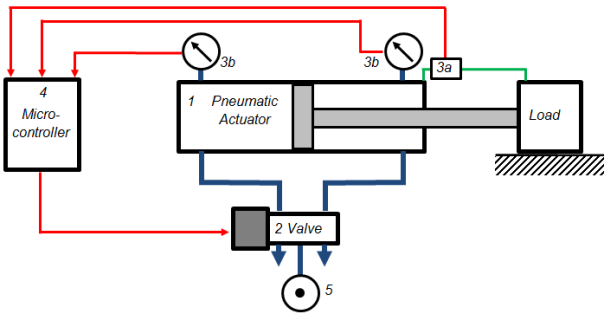

Figure 1.3.: Pneumatic actuation system scheme

A schematic diagram of the system under scope is shown in Figure 1.3. The double-sided pneumatic actuator (1) is pneumatically connected by two tubes to the 5/3 proportional directional control valve (2), and mechanically connected at the end of the actuator's rod to the external load. The position of the rod is measured by a potentiometer (3a), and pressures on both sides of the actuator are measured by two pressure gauges (3b). Data from the sensors are acquired by the micro-controller (4). The five ports of the valve are connected as follows: two ports are connected to the actuator, as mentioned, two ports exits to the atmosphere and one port is connected by tube to the pneumatic source (5), which is a comprehensive term for a system comprising a compressor, air filter, dryer, pressure regulator, and capacitive tube.

1.4. Thesis Outline and Contributions

We start with the dynamical model of the actuator in Chapter 2. The main subject of this chapter is the derivation of the actuator's equation of motion, but we also describe its general operation principals. We briefly introduce the concept of the Lagrangian and the Euler-Lagrange equation of motion, and we derive the potential and kinetic energy of the actuator. Finally, we conclude with an analytical analysis of the model.

The contribution of Chapter 2 is the exclusive methodology used to model the actuator. While previous papers base their dynamical model on Newton's

second law, we adopt the classical method of energetic considerations to describe the dynamics of the actuator. Instead of analyzing the forces acting upon the piston of the actuator, we define the mechanical kinetic energy and the pneumatic potential energy of the actuator, and combine them to derive the the multi-domain Lagrangian of the actuator. The Lagrangian of the actuator is also an innovative concept that is used for the derivation of the Euler-Lagrange equation of motion.

Chapter 3 is dedicated to control. We apply the nonlinear backstepping method and design a state feedback control law to stabilize the system. The tracking problem is also addressed.

The contribution of Chapter 3 lies in the choice of control parameter; although we intend to control the position of the actuator, we use the derivative of the potential energy as the control parameter. The resulted control law allows tracking a position trajectory reference while the actuator is subjected to an external force with a magnitude that varies between 500 to 1200[N].

Chapter 4 includes a comparison between simulation of the actuator to measurements of the real actuator, and tracking test results conducted on a designated test rig. The final chapter, Chapter 5, concludes the thesis.

The work done to accomplish this thesis goal is complete in an academic and engineering sense. To maintain a logical order of reading, only the academic aspect is described in the chapters, though much more was done. Other important issues, such as the modeling of the flow-rate through the valve and the a description of the test rig, appear in the appendixes. Issues like planning and manufacturing of the test rig, measurement equipment, experiment planning, data acquisition, implementation and data analysis methodology, are not included in this paper.

The last contribution of this thesis, found in appendix D, is the innovative method for modeling the mass flow-rate of air passing through the valve. By this method, we adopt an experimental identification approach in order to develop a three-dimensional model of the flow-rate as a function of the input to the valve and the pressure in its ports.

2. Pneumatic Actuator Dynamical Model

The pneumatic actuator is an element that transforms pneumatic energy into mechanical work. Pneumatic energy is the energy stored in pressurized compressible fluid (mostly air), and mechanical work is the product of the force exerted by the actuator and the actual motion done as a result of this force. This chapter deals with an analysis of the actuator's dynamics and the derivation of a mathematical model that describes its motion.

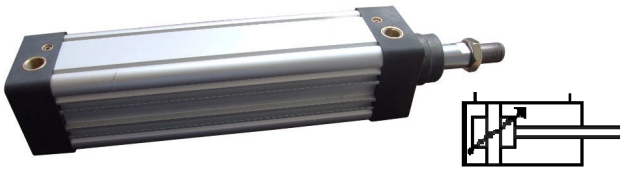

Figure 2.1.: Pneumatic actuator and its schematic symbol

2.1. General Operation

The actuator under scope is of a double-sided single-ended piston rod type. Figure 2.1 includes an actuator and its schematic symbol, which illustrates the basic structure of the actuator. It is comprised of a cylinder and a piston, which separates the inner volume into two chambers. Two ports at the ends of the cylinder allow air charge or discharge from the chambers. Changing the mass of air in the chamber, which alters the pressure in it, thus change the net force acting on the piston and therefore causes movement of the piston and the connected rod. A detailed schematic representation of the actuator

is shown in Figure 2.2. In this figure, parameters subtitled with the index $i = 1, 2$ correspond to chamber i. That is, $\dot{m}_i$ is the inlet or outlet mass flow-rate through the port of chamber i; A_i is the piston cross section from the side of chamber i; P_i is the pressure in the chamber; m_i is the mass of air in the chamber and V_i is volume of the chamber; M represents the total mass of the piston, the rod, and the load connected to the end of the rod; and, F_{ex} is the external force. There are two pairs of triangles at the ends of the cylinder; the two upper triangles represent the inlet/outlet ports and the two lower black triangles indicate a 'dead volume' that remains even when the piston reaches the end of the stroke.

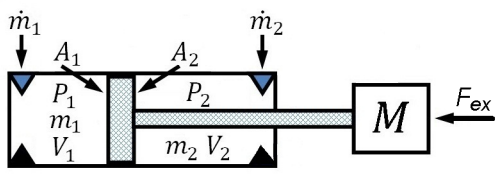

Figure 2.2.: Pneumatic actuator scheme with the descriptive parameters

2.2. Dynamics Modeling

The common approach to model pneumatic actuation system, which was established by Shearer in 1954 [3], integrates the actuator dynamics described by Newton's second law and the model of the mass flow-rate through the valve into one model. Actually, all the papers and books we have encountered in the field of pneumatic actuation use this approach, with only different simplifying assumptions (such as, the working gas obeys the ideal gas equation of state: $PV = mRT$), resulting in different versions of the original model. While Shearer's model is linear and is valid only for small movements away from the actuator center position, later works extended the model to be valid for the whole actuator stroke, and most of the papers published in the last

two decades propose much more accurate models with different levels of non-linearity (for example, see Richer and Hurmuzlu [4]).

In this thesis we introduce an original approach to the modeling of the pneumatic system. First we leave the mass flow-rate through the valve and focus only on the actuator. Then, we adopt a different perspective on the method of analyzing the actuator dynamics. Instead of using the traditional force analysis, we derive the actuator model based on energy analysis. That is, we derive the kinetic energy and potential energy, combine them to formulate the Lagrangian of the actuator, and then by using the Euler-Lagrange equation we reach the desired equation of motion.

The rest of this chapter is as follows: A fundamental framework to the modeling of the actuator using energy considerations is provided in section 2.3. Then we define the kinetic energy of the actuator, in section 2.4, and the potential energy of the actuator, in section 2.5. In section 2.6 the friction is taken into consideration, and section 2.7 deals with the external force acting on the piston rod. In section 2.8 we combine all the energy elements to form the Lagrangian of the actuator and the Euler-Lagrange equation of motion. The last section, 2.9, is dedicated to the analysis of the actuator's model.

2.3. Fundamentals of Energy Modeling

The objective of this chapter is to derive a mathematical expression for the actuator dynamics. In this section we briefly introduce the concept, taken from the classical mechanics, and apply it to modeling of a physical system from the perspective of energy.

Definition. Lagrangian[5] The Lagrangian is the **difference** between the total kinetic energy, $\mathcal{T}$, associated with the masses and moments of inertia and the total potential energy, $\mathcal{V}$, associated with gravitational forces and stiffness elements.

The Lagrangian, $\mathcal{L}$, is defined by

$$\mathcal{L} = \mathcal{T} - \mathcal{V}. \tag{2.1}$$

The kinetic energy is discussed in section 2.4 and the potential energy is in section 2.5.

The Euler-Lagrange equation of motion (also referred to as just Lagrange equation) as given by Goldstein [6]

$$\frac{d}{dt}\left(\frac{\partial \mathcal{L}}{\partial \dot{x}}\right) - \frac{\partial \mathcal{L}}{\partial x} = 0\,, \tag{2.2}$$

where x is the state of the system, t is the time, and $\dot{x} = \frac{dx}{dt}$ is the time derivative of x. Regarding the actuator, x and $\dot{x}$ represent the displacement and the velocity of the piston, respectively.

Since the actuator is subjected to energy dissipation, $\mathcal{F}$, and external forces, F_{ex}, we write a general form of the Euler-Lagrange equation of motion

$$\frac{d}{dt}\left(\frac{\partial \mathcal{L}}{\partial \dot{x}}\right) - \frac{\partial \mathcal{L}}{\partial x} = -\frac{\partial \mathcal{F}}{\partial \dot{x}} - F_{ex}\,, \tag{2.3}$$

where $\frac{\partial \mathcal{F}}{\partial \dot{x}}$ is the partial derivative of the energy dissipation with respect to the velocity. The energy dissipation in the actuator is due to work done by the friction force, which is analyzed in section 2.6. The external force that acts on the piston rod, F_{ex}, was added only for the completeness of the equation. We do not model the external force, but since it is the major disruption to the control effort, we include a general characterization in section 2.7. In the pneumatic system under scope, the external force is not directly measured, though it can be we evaluate by the pressure measurements.

2.4. Kinetic Energy

The kinetic energy of the actuator, $\mathcal{T}$, refers to the energy content of the movement of the piston, rod, and external load, i.e., the moving mass

$$\mathcal{T} = \frac{p^2}{2M}\,, \tag{2.4}$$

where M is the moving mass and p is the momentum of this mass. Since the relation between momentum and velocity is $p = M\dot{x}$, one can write the

kinetic energy [5], $\mathcal{T}$, which is used in the Lagrangian,

$$\mathcal{T} = \frac{1}{2} M \dot{x}^2. \tag{2.5}$$

2.5. Potential Energy

The first step towards deriving the potential energy is to determine the relation between the force and the generalized displacement in the pneumatic domain. Jeltsema and Scherpen [5] suggested that the pressure is analogue to the force and the volume is the generalized displacement in the pneumatic domain.

2.5.1. The Relation Between Pressure and Volume

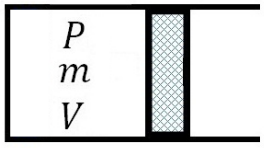

Figure 2.3.: Varying volume chamber

Consider a simple case of a varying volume chamber, as displayed in Figure 2.3. The chamber is sealed by the cylinder walls and a movable piston. We define P as pressure of the air inside the chamber, m is the mass of air in the chamber, and V is the volume. Assuming the air behaves as an ideal gas[1], the relation between pressure and volume is defined by the ideal gas law

$$PV = mRT\,. \tag{2.6}$$

[1]The air can be considered as an ideal gas if the compressibility factor, Z, is close to unity. Though the compressibility changes with pressure and temperature, we can limit the working condition of the air in the pneumatic system under scope to temperatures of $280 \div 350\,[K]$ and pressures of $1 \div 10\,[Bar]$ ($1\,[Bar] = 100000\,[Pa]$). Under these conditions, the compressibility factor is $0.998 \leq Z \leq 1.001$ and the ideal gas assumption is reasonable. In fact, this is an assumption taken in all the related papers we have encountered.

where R is the specific gas constant of air and T is the air temperature.

2.5.2. Isothermal Process

The thermodynamical process taking place inside the pneumatic chamber includes compression, expansion, charging, and discharging of air into and out of the chamber; therefore, it certainly involves temperature changes. Shearer [3], for instance, attributes the charging process as adiabatic (zero heat transfer) and the discharging process as isothermal (constant temperature). Richer and Hurmuzlu [4] enhanced shearer's approach by claiming that the thermal characteristic of the compression/expansion process is better described using a poly-tropic process, due to the piston movement. The adiabatic, isothermal and poly-tropic processes are defined in appendix A. Beater [1] included in his book a broaden description of the thermal process covering isothermal, adiabatic and poly-tropic processes, though he eventually applied the isothermal process to derive the control law. Beater also cited Kawakami et al. [7], who showed that even though the temperature dynamics inside the actuator's chambers are neglected, and temperature is assumed constant, adequate model accuracy is achieved.

To conclude the discussion on the thermodynamic process, it should be noted that an intensive description of the heat transfer process is out of the scope of this thesis. Relating to all the above mentioned sources, we consider the isothermal process as an appropriate assumption.

2.5.3. Potential Energy of a Varying Volume Chamber

Considering the isothermal process assumption taken in the previous subsection, we define an increment of work done by pressure

$$PdV = \frac{mRT}{V}dV\,. \tag{2.7}$$

The total work done by the pressure is the integral

$$W = -\int_{V_0}^{V} PdV = -mRTln\left(\frac{V}{V_0}\right), \tag{2.8}$$

where V_0 is the initial volume (or dead volume[2]), as shown in Figure 2.4. The minus sign in (2.8) is a result of sign convection, by which mechanical work done by the system on the surroundings is taken as negative.

2.5.4. Potential Energy of the Actuator

Extending the case of the varying volume chamber, in this subsection the idea of potential energy is implemented on a closed volume container that is divided into two chambers by a piston, as shown in Figure 2.4. This container is similar to a sealed actuator for which the potential energy, $\mathcal{V}$, is a function of the chamber's volume. That is

$$\mathcal{V}(V_1, V_2) = -RT\left[m_1 ln\left(\frac{V_1}{V_{0,1}}\right) + m_2 ln\left(\frac{V_2}{V_{0,2}}\right)\right], \tag{2.9}$$

where m_i , V_i, and $V_{0,i}$ are the mass of air, the volume, and the initial volume of chamber i, respectively. The dead volume of the actuator under scope is reported as equal for both chambers, therefore it can be replaced with the sign V_0.

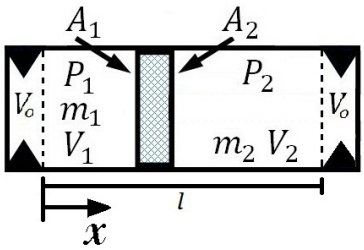

Figure 2.4.: Closed volume container separated into two chambers by a piston

[2]The minimum volume left when the piston reaches the end of the stroke is referred to as 'dead volume'. It has a constant value, usually declared in the manufacturer's manual.

The relations between the volumes and the piston's position is

$$V_1 = A_1 x,\ V_2 = A_2 (l - x) . \tag{2.10}$$

Substituting V_0 and (2.10) into (2.9), we have

$$\mathcal{V}(x) = -RT \left[m_1 ln \left(\frac{A_1 x}{V_0} \right) + m_2 ln \left(\frac{A_2 (l - x)}{V_0} \right) \right] . \tag{2.11}$$

Since the masses of air m_1 and m_2 are constant, (2.11) indicates that the potential energy is dependent only on the generalized displacement of the piston, x.

Remark. Concerning the realistic unsealed actuator, we know that the masses m_1 and m_2 are also state parameters, since at any time they can be changed by inlet or outlet flow controlled by the valve. Nevertheless, since we can measure the pressures in the chambers of the actuator, with a high frequency, and then calculate the current masses, we will ignore the mass flow-rate dynamics. This allows us to treat the masses, for a specific time frame, as constants and assume that position and velocity are the only state parameters. We continue with the assumption of the constant masses throughout this chapter.

Example 2.1. We want to simulate the potential energy of the actuator for the whole range of the piston stroke, i.e. for $0 < x < 0.3$. First we define all the parameters according to equation 2.11. We Start from the known parameters, i.e.: piston stroke - $l = 0.3\,[m]$, piston diameter - $D = 0.063\,[m]$, piston rod diameter - $D_r = 0.02\,[m]$, and dead volume - $V_0 = 18e^{-6}\,[m^3]$. Now the piston cross section can now be calculated:

$$A_1 = \frac{\pi D^2}{4} = 3.1e^{-3}\left[m^2\right], \quad A_2 = \frac{\pi (D^2 - D_r^2)}{4} = 2.8e^{-3}\left[m^2\right] .$$

The specific gas constant of air is $R = 287\,[\mathrm{J/kg{-}K}]$. Other parameters are chosen arbitrarily: ambient pressure - $P_{atm} = 100\,[kPa]$ and ambient temperature - $T = 298\,[K]$; the initial masses of air in the chambers are $m_1 = m_2 = 5e^{-4}\,[kg]$. Figure 2.5 shows the solution $\mathcal{V}(x)$ for the whole range of the piston stroke.

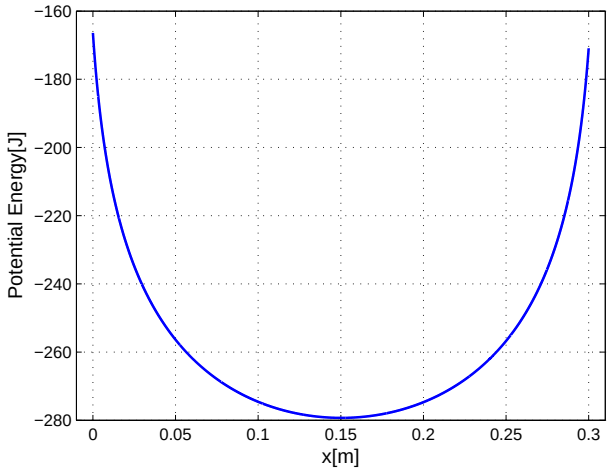

Figure 2.5.: The potential energy of the actuator as a function of the displacement

Conclusions:

- The simulated potential energy behaves as a positive quadratic function with a global minimum. The horizontal location of the minimum is at $x = \bar{x} = 0.15[m]$. This minimum potential energy, $\mathcal{V}_{min} = \mathcal{V}(\bar{x})$ is the equilibrium point of the actuator for the given masses of air in the chambers. Choosing different masses will affect the horizontal location of the equilibrium point.

- Although the vertical position of $\mathcal{V}_{min}$ is also a result of the chosen conditions, its definition as a quantity of energy indicate that $\mathcal{V}$ is a scalar which depends on the absolute quantities of the temperature and pressures. Since the last two are arbitrary (or historically) per-scaled according to international standards, and since energy is defined as a positive quantity, with its theoretical minimum at 0, the vertical location of $\mathcal{V}_{min}$ is insignificant and can be shifted to any desired location on the vertical axis. This last conclusion can be exploited for stability analysis.

2.6. Friction

Energy loss due to friction in the actuator is caused by the seal around the piston and the seal between the rod bore and the rod. The seals are designed to prevent compressed air leakage from one chamber to the other, and also escaping from the actuator to the outside. Though friction force can significantly influence the dynamics of the actuator, manufacturers usually include minimal information about it in the manuals. Several friction models can be found in literature. For example, in his book Beater [1] introduced and compared a few of the common models associated with pneumatic actuators, although for the control design purpose he used a linear model of velocity dependent friction force.

Concentrating on the thesis subject, i.e. control, we adopt the simple continuous linear model of viscous friction. That is

$$F_f(\dot{x}) = \mu_v \dot{x}\,, \tag{2.12}$$

where $\dot{x}$ is the piston velocity and μ_v is the viscous friction coefficient.

We want to define the energy dissipation due to friction in the actuator, $\mathcal{F}(\dot{x})$. It is defined by the integral

$$\mathcal{F}(\dot{x}) = \int_0^{\dot{x}} F_f(\dot{x})\, d\dot{x} = \frac{1}{2}\mu_v \dot{x}^2 \tag{2.13}$$

and represent the rate of the change in work done by the friction force, thus it has the units of power. Recalling the Euler-Lagrange equation 2.3, we calculate $\frac{\partial \mathcal{F}}{\partial \dot{x}}$, which is the partial derivative of $\mathcal{F}(\dot{x})$, and arrive at

$$\frac{\partial \mathcal{F}}{\partial \dot{x}} = \frac{\partial}{\partial \dot{x}}\left(\frac{1}{2}\mu_v \dot{x}^2\right) = \mu_v \dot{x}\,. \tag{2.14}$$

Remark. Despite the simplistic viscous friction model, experiment results included in Chapter 4 show that the dynamic model is adequately accurate. Moreover, this simplicity has a significant advantage in the implementation of real-time control algorithms and in simulation programming.

2.7. External Force

The only element in the Euler-Lagrange equation we do not explicitly define is the external force acting on the piston rod, i.e. F_{ex}, which plays the roll of a time varying disruption. Although we do not directly measure it, we design, in Chapter 3, a the controller that can overcome its effect. Nevertheless, we mention two general characteristics of F_{ex}:

1. It acts only in the longitudinal axis[3];
2. Its magnitude can vary continuously between 0 [N] to a maximum of 1500 [N].

These characteristics arise from the system designation, to be integrated into the walking robot, introduced in Chapter 1. In our attempt to imitate the robot's environment, we know that its own weight, gravity, and inertia, are the cause for the real F_{ex}.

2.8. The Lagrangian of the Actuator

We derive the Lagrange equation of motion of an ideal actuator, which is a frictionless actuator that acts under zero external force. Substituting the kinetic energy (2.4) and the potential energy (2.11) into the Lagrangian (2.1) yields

$$\mathcal{L}(x,\dot{x}) = \frac{1}{2}M\dot{x}^2 - RT\left[m_1 ln\left(\frac{A_1 x}{V_0}\right) + m_2 ln\left(\frac{A_2(l-x)}{V_0}\right)\right]. \tag{2.15}$$

Executing the derivatives in the Euler-Lagrange equation (2.2) results in

$$M\ddot{x} - RT\left(\frac{m_1}{x} - \frac{m_2}{l-x}\right) = 0\,, \tag{2.16}$$

which is the equation of motion of an ideal actuator. Adding the friction force from (2.12), we get the final form of the Euler-Lagrange equation of motion

[3]The actuator is designed to allow a movement along the longitudinal axis only.

of the actuator,

$$M\ddot{x} - RT\left(\frac{m_1}{x} - \frac{m_2}{l-x}\right) = -\mu_v \dot{x}\,. \tag{2.17}$$

2.9. Dynamic Model Analysis

In this section we analyze the dynamical model of the actuator in order to gain a better understanding of its behavior as a preliminary step before we design its control. First we transform the equation of motion into state space form in subsection 2.9.1. We continue and calculate the fixed point of the actuator in subsection 2.9.2, and finish by exploring the stability of the linearized model using phase portrait in subsection 2.9.3.

2.9.1. State Space Form

Until now the actuator's dynamics have been described by the Euler-Lagrange equation of motion, which is a second degree differential equation. In this section we use the state space form - a first degree differential equation which will be the basis for the dynamic model analysis and the control design.

We start with the Euler-Lagrange equation of motion (2.17)

$$M\ddot{x} - RT\left(\frac{m_1}{x} - \frac{m_2}{l-x}\right) + \mu_v \dot{x} = 0\,,$$

where x is the displacement of the piston, M is the total mass connected to the piston, R is the gas constant of air, T is the air temperature, m_1 and m_2 are the masses of air in the two chambers of the actuator, l is the piston stroke, μ_v is the viscous friction coefficient, and $\dot{x}$ is the velocity. The change of variables, $x_1 = x$ and $x_2 = \dot{x}$, leads to

$$M\dot{x}_2 - RT\left(\frac{m_1}{x_1} - \frac{m_2}{l-x_1}\right) + \mu_v x_2 = 0\,.$$

Rearranging in the state space form, i.e. $f(\mathbf{x}) = \dot{\mathbf{x}}$, where $\mathbf{x} = [x_1, x_2]^T$ is the

state vector, we have

$$f(\mathbf{x}) = \begin{bmatrix} \dot{x}_1 \\ \dot{x}_2 \end{bmatrix} = \begin{bmatrix} x_2 \\ \frac{1}{M}\left(RT\left(\frac{m_1}{x_1} - \frac{m_2}{l-x_1}\right) - \mu_v x_2\right) \end{bmatrix}. \tag{2.18}$$

2.9.2. Fixed Point

We calculate the fixed point, $\bar{\mathbf{x}}$, by solving $f(\bar{\mathbf{x}}) = 0$. That is,

$$\begin{bmatrix} x_2 \\ \frac{1}{M}\left(RT\left(\frac{m_1}{x_1} - \frac{m_2}{l-x_1}\right) - \mu_v x_2\right) \end{bmatrix}_{\mathbf{x}=\bar{\mathbf{x}}} = \begin{bmatrix} 0 \\ 0 \end{bmatrix}$$

and the solution is the desired fixed point,

$$\bar{\mathbf{x}} = (\bar{x}_1, \bar{x}_2) = \left(\frac{m_1 l}{m_1 + m_2}, 0\right). \tag{2.19}$$

From the last equation we see that the position of the fixed point, $\bar{x}_1$, is dependent on m_1 and m_2.

Example 2.2. We want to calculate the fixed point of the actuator for a specific state defined by the data given in example 2.1. Starting by choosing an arbitrary initial position, $x(t=0) = x_0 = 0.15\,[m]$, we then calculate the initial volume of the chambers by multiplying it in the piston's cross section and adding the dead volume, $V_0 = 1.8e^{-6}\,[m^3]$. The initial volume of chamber 1 is

$$V_1 = x_0 \frac{\pi D^2}{4} + V_0 = 4.86e^{-4}\left[m^3\right]$$

and the initial volume of chamber 2 is

$$V_2 = (l - x_0)\frac{\pi\left(D^2 - D_r^2\right)}{4} + V_0 = 4.38e^{-4}\left[m^3\right].$$

Now, we calculate the mass of air in the chambers, m_1, m_2, using the ideal gas law (2.6) with an arbitrary initial chamber pressure, $P_1 = P_2 = 100,000\,[Pa]$. The mass of air in chamber 1:

$$m_1 = \frac{P_{atm} V_1}{RT} = 5.68e^{-4}\,[kg].$$

Mass of air in chamber 2:

$$m_2 = \frac{P_{atm} V_2}{RT} = 5.13e^{-4}\,[kg]\,.$$

Recalling that the velocity of the fixed point is zero ($\bar{x}_2 = 0\,\left[\frac{m}{s}\right]$), we can calculate the position fixed point, $\bar{x}_1$, which is actually the equilibrium position for the given situation,

$$\bar{x}_1 = \frac{m_1 l}{m_1 + m_2} = 0.1576\,[m]\,.$$

2.9.3. Phase Portrait

One of the most important characteristics engineers need to know about the system for which the controller is designed, is the stability (see appendix B for stability definitions). In order to explore the stability of the actuator we use the phase portrait, which is an illustration of a solution of the actuator dynamics for some specific initial conditions. The solution is plotted on a graph of the velocity versus the position of the actuator. Figure 2.6 displays the solution of the dynamical system for two cases; a frictionless actuator, i.e. (2.16), and an actuator influenced by friction according to (2.17). The initial velocity is set to $x_2 = 2.5\,\left[\frac{m}{s}\right]$, the initial position is $x_1 = 0.15\,[m]$, and all the other system conditions and parameters are equal to those given in example 2.2.

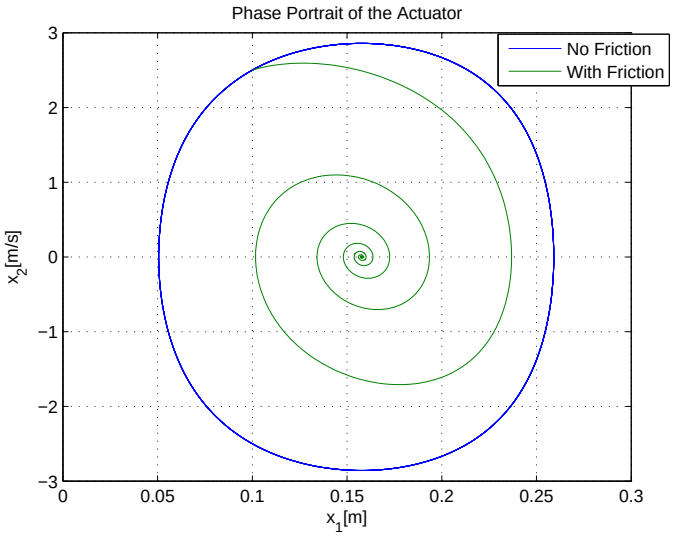

Figure 2.6.: The phase portrait of the actuator, with and without friction

Examining the results of the frictionless actuator, i.e. the blue curve, the image of a periodic solution in the phase portrait is a closed trajectory, which is usually called a periodic orbit or a closed orbit. The equilibrium, however, is not asymptotically stable, since trajectories starting off the equilibrium point do not tend to it eventually [8]. Thus, we conclude that the frictionless actuator has a stable equilibrium point at $\bar{\mathbf{x}} = (\bar{x}_1, \bar{x}_2) = (0.158, 0)$. This periodic orbit is a result of a constant energy level which does not dissipate, since there is no friction. When friction is taken into consideration (the green curve), trajectories starting close to the equilibrium point tend to it as time tends to infinity, therefore we conclude that $\bar{\mathbf{x}}$ is an asymptotic stable equilibrium point of the actuator.

3. Control

Pneumatic systems have been treated by engineers in a controversial manner for many years. Their main advantages, such as high power to weight ratio, cleanliness, low cost, reliability, and a simple mechanism, have contributed to their widespread throughout the industry, especially in automation and actuation fields. On the other hand, compressibility of the working media (usually air), complex friction behavior, and nonlinear flow through the valve make it difficult to accurately anticipate their dynamic behavior. This disadvantage traditionally restricts the development effort of open-loop applications, where accurate motion control is not required.

For example, a combination of pneumatic actuator, switching valve, and mechanical stops will probably be the first choice of an engineer who wants to solve a transportation problem, such as moving some part from one point to another. Usually, when more than two stops are needed or if a specific velocity profile is required, then pneumatics is abandoned and electronic or hydraulic systems are favored, since these are easier to control. Pneumatic systems require sophisticated control methods and modern computation capabilities, which were not available up until the last three decades.

The first results of closed-loop position controlled pneumatic systems were presented in 1954 by Shearer [3]. His work included a theoretical analysis of the pneumatic actuator and of the proportional directional control valve, experimental results, and simulation performed on an analog computer. Based on his linearized model, Shearer introduced a controller that could stabilize the system at the equilibrium point. This control solution was valid only if the actuator's initial position was in proximity to the middle of the stroke, i.e., close to the equilibrium point.

Throughout the 60s to the 90s of the previous decade, pneumatic control

significantly advanced through the use of various tools from linear control theory. Beater [1] reviewed some important contributions such as: Burrows and Webb (1966) who extended Shearer's analysis using the rootlocus technique, Barker (1976) who used the Luenberger observer to reconstruct the velocity and acceleration from the measured position signal; and Heinen (1976), found that the single loop proportional position control could be dramatically improved by the use of additional signals, such as the pressure. Other interesting ideas can be found in the publication of Wang et al. (1999) [9], who integrated proportional, differential, and acceleration feedback with velocity feedforward, or the control strategy proposed by Lai et al. (1990) [10] which uses PWM (pulse width modulation) of on-off valve (instead of the conventional proportional direction control valve) controlled actuators.

Recent advancements in computational capabilities, which allow for solving more complex equations faster and with higher accuracy, have led to a new phase in pneumatic control. In the last two decades we have seen the growing interest in nonlinear control theory and its application to pneumatics. Richer and Hurmuzlu [4, 11] introduced in 2000 the sliding mode method to force control their system. They used a highly nonlinear model that included unusual effects of leakage between the actuator's chambers, time delay and attenuation in the pneumatic lines, as well as the obvious effects of flow through the valve, air compressibility in cylinder chambers, and the end of stroke inactive volume. In 2006 Rao et al. [12] applied the backstepping methodology to position control a small pneumatic actuator.

This chapter deals with the design of a state feedback control law that will stabilize the pneumatic actuator and allow tracking of a desired position trajectory. The control law is designed such that it take into consideration the nonlinear dynamics of the pneumatic system and a disturbance of a time varying external force.

The chapter is organized as follows: We start, in section 3.1, with motivation for choosing our control strategy, the backstepping method. In Sections 3.2 and 3.3 we formulate the control problem in terms of the backstepping method. Sections 3.4-3.6 introduce the implementation of the backstepping technique on the pneumatic system and the derivation of the state feedback

control law.

3.1. Choosing a Control Strategy

The decision of which control strategy to implement is influenced by the following considerations:

1. We want to utilize the nonlinear dynamical model of the actuator, derived in Chapter 2. Therefore, a nonlinear control strategy is preferred.

2. The control strategy should apply to the special structure of the pneumatic actuator's dynamic model, as seen in Figure 3.1. In the pneumatic system, the input to the actuator, the mass flow-rate, $\dot{m}_1$ and $\dot{m}_2$, are integrated to be the mass of air, m_1 and m_2. The latter are members of the dynamic model's equation (2.17).

3. If treated separately, the inner loop that represents the friction dynamics of the actuator, i.e., $\ddot{x} = \dot{x}\frac{\mu_v}{M}$, is a relatively simple system to control.

The backstepping method applies to those considerations.

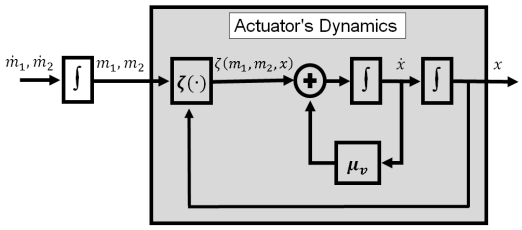

Figure 3.1.: A block diagram of the pneumatic actuator's dynamics

The backstepping technique was developed circa 1990 by Petar V. Kokotovic and others for designing stabilizing controls for a special class of nonlinear dynamical systems. These systems are built from subsystems that radiate out from an irreducible subsystem that can be stabilized using some other method. Because of this recursive structure, the designer can start the design process at the known-stable system, and then "back out" new controllers that progressively stabilize each outer subsystem. The process terminates

when the final external control is reached. Hence, this process is known as backstepping [13].

3.2. Formulation

We start with our system, the actuator's dynamic model (2.18), as derived in Chapter 2:

$$\dot{x}_1 = x_2 \tag{3.1}$$

$$\dot{x}_2 = \frac{1}{M}\left(RT\left(\frac{m_1}{x_1} - \frac{m_2}{l - x_1}\right) - \mu_v x_2\right). \tag{3.2}$$

Denoting ζ as the derivative of the potential energy,

$$\zeta = RT\left(\frac{m_1}{x_1} - \frac{m_2}{l - x_1}\right), \tag{3.3}$$

we can write

$$\dot{x}_1 = x_2 \tag{3.4}$$

$$\dot{x}_2 = \frac{1}{M}\left(\zeta - \mu_v x_2\right). \tag{3.5}$$

Notice that the dynamic model is an autonomous system which has no specified input. Therefore, we expand the model with the time derivative of ζ, i.e.,

$$\begin{aligned}\frac{d\zeta}{dt} &= \frac{\partial\zeta}{\partial m_1}\frac{dm_1}{dt} + \frac{\partial\zeta}{\partial m_2}\frac{dm_2}{dt} + \frac{\partial\zeta}{\partial x_1}\frac{dx_1}{dt} + \frac{\partial\zeta}{\partial x_2}\frac{dx_2}{dt} \\ &= RT\left(\frac{\dot{m}_1}{x_1} - \frac{\dot{m}_2}{l - x_1} - x_2\left(\frac{m_1}{x_1^2} + \frac{m_2}{(l - x_1)^2}\right)\right),\end{aligned} \tag{3.6}$$

where $\dot{m}_1$ and $\dot{m}_2$ are the mass flow-rate of air entering and exiting the chambers of the actuator. The mass flow-rate is the input to the actuator and it is, in itself, controlled by the input to the valve. For control design purposes,

we use a linear model to describe the mass flow-rate through the valve[1]:

$$\dot{m}_1 = \alpha_1 u_V + \beta_1 \tag{3.7}$$
$$\dot{m}_2 = -\alpha_2 u_V + \beta_2 \,, \tag{3.8}$$

where α_1, α_2, β_1 and β_2 are all positive scalars that characterize the flow and u_V is the voltage input of the valve. From experiment identification we acquire $\alpha_1 = -\alpha_2 = -0.004736$[kg/s-V] and $\beta_1 = \beta_2 = 0.0005$[kg/s].

Substituting (3.7) and (3.8) into (3.3), and adding (3.3) to system (3.4)-(3.5) as the third equation, we get a comprehensive pneumatic actuation model that includes the valve input u_V,

$$\dot{x}_1 = x_2 \tag{3.9}$$
$$\dot{x}_2 = \frac{1}{M}\left(\zeta - \mu_v x_2\right) \tag{3.10}$$
$$\dot{\zeta} = RT\left(\left(\frac{\alpha_1}{x_1} - \frac{\alpha_2}{l - x_1}\right) u_V + \cdots + \frac{\beta_1}{x_1} - \frac{\beta_2}{l - x_1} - x_2\left(\frac{m_1}{x_1^2} + \frac{m_2}{(l - x_1)^2}\right)\right). \tag{3.11}$$

System (3.9)-(3.11) is in the strict-feedback form[2] which is suitable for the backstepping method. The transformation

$$u_V = \frac{1}{\left(\frac{\alpha_1}{x_1} - \frac{\alpha_2}{l - x_1}\right)}\left(-\frac{\beta_1}{x_1} + \frac{\beta_2}{l - x_1} + x_2\left(\frac{m_1}{x_1^2} + \frac{m_2}{(l - x_1)^2}\right) + \frac{u}{RT}\right) \tag{3.12}$$

yields the representation

$$\dot{x}_1 = x_2 \tag{3.13}$$
$$\dot{x}_2 = \frac{1}{M}\left(\zeta - \mu_v x_2\right) \tag{3.14}$$
$$\dot{\zeta} = u. \tag{3.15}$$

[1] See Appendix D for an extensive inquiry of the mass flow-rate through the valve.
[2] See Appendix B.1 for the definition of the strict-feedback form

Furthermore, by defining

$$f = \begin{bmatrix} x_2 \\ -\frac{\mu_v}{M} x_2 \end{bmatrix} \tag{3.16}$$

and

$$g = \begin{bmatrix} 0 \\ \frac{1}{M} \end{bmatrix}, \tag{3.17}$$

we transform (3.13)-(3.15) into the single integrator system

$$\dot{\mathbf{X}} = f(\mathbf{X}) + g(\mathbf{X})\,\zeta \tag{3.18}$$

$$\dot{\zeta} = u\,, \tag{3.19}$$

where $\left[\mathbf{X}^T, \zeta\right]^T \in \mathbb{R}^3$ is the state vector and $u \in \mathbb{R}$ is the control input. We apply the backstepping procedure on the single integrator system (3.18)-(3.19). Further requirements are: functions $f : D \to \mathbb{R}^2$, and $g : D \to \mathbb{R}^2$ are smooth in a domain $D \in \mathbb{R}^2$ that contains $\mathbf{X} = \mathbf{0}$; $f(\mathbf{0}) = \mathbf{0}$, and $g(\mathbf{X}) \neq \mathbf{0}$.

A block diagram that represents system (3.18)-(3.19) is shown in Figure 3.2; ζ is the input to the first component represented by (3.18) and the component represented by (3.19) is the integrator. Comparing Figure 3.1 with Figure 3.2, we notice that the structure of the pneumatic system resembles that of the single integrator system (3.18)-(3.19).

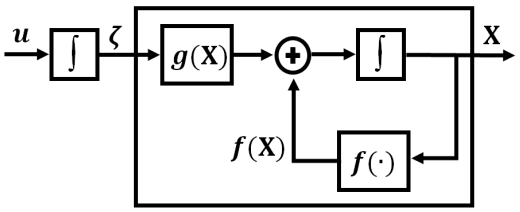

Figure 3.2.: Block diagram of the system 3.18-3.19

The objective of the backstepping method is to design a state feedback control law to stabilize the origin ($\mathbf{X} = \mathbf{0}, \zeta = 0$). Thus, the origin ($\mathbf{X} = \mathbf{0}, \zeta = 0$) must be an equilibrium point of the system. According to (3.16), $f(\mathbf{0}) = \mathbf{0}$

for $x_2 = 0$, but according to (3.3), in order to have $\zeta = 0$ we need to solve

$$RT\left(\frac{m_1}{x_1} - \frac{m_2}{l - x_1}\right) = 0.$$

Thus, we find that the equilibrium is located at

$$x_1 = \bar{x}_1 = \frac{m_1 l}{m_1 + m_2},$$

where $\bar{x}_1$ is the equilibrium position of the actuator, which is a function of the masses, m_1 and m_2. The fact that $\bar{x}_1$ is not necessarily located at the origin (i.e. $\bar{x}_1 \neq 0$) is inconsistent with the initial requirements, but we can change variables to shift $\bar{x}_1$ to the origin. For example, consider the system $\dot{\mathbf{Y}} = h(\mathbf{Y})$, where $h\left(\bar{\mathbf{Y}}\right) = \mathbf{0}$, $\bar{\mathbf{Y}} = [\bar{y}, \dot{\bar{y}}]^T$ and $\bar{y} \neq 0$. Now, define a change of variable $\hat{y} = y - \bar{y}$. The derivative of $\hat{y}$ is

$$\dot{\hat{y}} = \dot{y},$$

and

$$h\left(\hat{\mathbf{Y}}\right) = \begin{bmatrix} y - \bar{y} \\ \dot{y} \end{bmatrix} \triangleq h'(\mathbf{Y}),$$

where $h'(\mathbf{0}) = \mathbf{0}$. With the new variable $\hat{\mathbf{Y}}$, the system has an equilibrium at the origin. Therefore, without loss of generality, we can assume that $h(\mathbf{Y})$ satisfies $h(\mathbf{0}) = \mathbf{0}$ and study the stability of the origin $\mathbf{Y} = \mathbf{0}$.
We conclude that, given the system (3.18)-(3.19) with the equilibrium point at

$$\left[\bar{\mathbf{X}}, \bar{\zeta}\right] = \left(\bar{x}_1, \bar{x}_2, \bar{\zeta}\right) = \left(\frac{m_1 l}{m_1 + m_2}, 0, 0\right),$$

if we choose a new state vector $\left[\hat{\mathbf{X}}, \hat{\zeta}\right] = \left(\hat{x}_1, \hat{x}_2, \hat{\zeta}\right)$, change variables such that $\hat{x}_1 = x_1 - \bar{x}_1$, and assume $u = 0$ at the origin, we get

$$\begin{aligned} \dot{\hat{X}} &= f\left(\hat{\mathbf{X}}\right) + g\left(\hat{\mathbf{X}}\right)\hat{\zeta} = \mathbf{0} \\ \dot{\hat{\zeta}} &= u = 0. \end{aligned}$$

Therefore, throughout this chapter we assume that the equilibrium point is at the origin, $\left[\hat{\mathbf{X}}, \hat{\zeta}\right] = (\mathbf{0}, 0)$.

3.3. The Tracking Problem

We wish to design a controller to track the position trajectory reference x_d. Since the backstepping method is designated to stabilize the system at the equilibrium point, we replace the state vector $[\mathbf{X}, \zeta]^T$ with the error state vector $[\mathbf{X}_e, \zeta_e]^T = (x_{e,1}, x_{e,2}, \zeta_e)^T$. The position tracking error, $x_{e,1}$, is

$$x_{e,1} = \hat{x}_1 - x_d. \tag{3.20}$$

The velocity error, $x_{e,2}$ is the time derivative of (3.20), i.e.,

$$x_{e,2} = \hat{x}_2 - \dot{x}_d \,, \tag{3.21}$$

where $\dot{x}_d$ is the time derivative of x_d. We also define the zeta error, ζ_e, by

$$\zeta_e = \zeta - \zeta_d \,, \tag{3.22}$$

where ζ_d is the desired derivative of the potential energy,

$$\zeta_d = RT \left(\frac{m_1}{x_d} - \frac{m_2}{l - x_d} \right).$$

We apply the backstepping method to the error dynamics system

$$\begin{aligned} \dot{x}_{e,1} &= x_{e,2} && (3.23) \\ \dot{x}_{e,2} &= \frac{1}{M} \left(\zeta_e - \mu_v x_{e,2} \right) && (3.24) \\ \dot{\zeta}_e &= u \,, && (3.25) \end{aligned}$$

such that u will stabilize the system at the origin ($\mathbf{X}_e = \mathbf{0}, \zeta_e = 0$), meaning that the error $x_{e,1}$ is eliminated and tracking x_d is achieved. System (3.23)-

(3.25) in the single integrator form is then

$$\dot{\mathbf{X}}_e = f(\mathbf{X}_e) + g(\mathbf{X}_e)\,\zeta_e \tag{3.26}$$

$$\dot{\zeta}_e = u. \tag{3.27}$$

3.4. Stability of the Subsystem

We begin with the first step of the backstepping method; suppose that the component (3.26) (we will refer to it as the subsystem) can be stabilized by a smooth state feedback control law $\zeta_e = \phi(\mathbf{X}_e)$, with $\phi(\mathbf{0}) = 0$. That is, the origin of

$$\dot{\mathbf{X}}_e = f(\mathbf{X}_e) + g(\mathbf{X}_e)\,\phi(\mathbf{X}_e) \tag{3.28}$$

is asymptotically stable. We want to find a Lyapunov function[3] $V(\mathbf{X}_e)$ whose derivative along the trajectories of the system is negative definite, i.e. $\dot{V}(\mathbf{X}_e) < 0, \forall \mathbf{X}_e \neq \mathbf{0}$. In other words, $V(\mathbf{X}_e)$ must satisfy the inequality

$$\frac{\partial V}{\partial \mathbf{X}_e}\left[f(\mathbf{X}_e) + g(\mathbf{X}_e)\,\phi(\mathbf{X}_e)\right] \leq -W(\mathbf{X}_e), \quad \forall \mathbf{X}_e \in D^2, \tag{3.29}$$

where $W(\mathbf{X}_e)$ is positive definite[4].

To explicitly define $\phi(\mathbf{X}_e)$ we choose a Lyapunov function

$$V(\mathbf{X}_e) = \frac{1}{2}\mathbf{X}_e^T\mathbf{X}_e,$$

and calculate the partial derivative of $V(\mathbf{X}_e)$ along the trajectories of the subsystem, that is

$$\frac{dV}{dt} = \frac{\partial V}{\partial \mathbf{X}_e}\frac{d\mathbf{X}_e}{dt}.$$

Since $\frac{d\mathbf{X}_e}{dt} = \dot{\mathbf{X}}_e$ is the state component of the subsystem, we substitute (3.28) to get

$$\frac{dV}{dt} = \frac{\partial V}{\partial \mathbf{X}_e}\left[f(\mathbf{X}_e) + g(\mathbf{X}_e)\,\phi(\mathbf{X}_e)\right].$$

[3] See Appendix B for the Lyapunov stability criterion
[4] See Appendix B for positive definite definition

Executing the derivatives and using (3.16) and (3.17), we get

$$\begin{aligned}
\frac{dV}{dt} &= \begin{pmatrix} \frac{\partial V}{\partial x_{e,1}} & \frac{\partial V}{\partial x_{e,2}} \end{pmatrix} \left[\begin{pmatrix} x_{e,2} \\ -\frac{\mu_v}{M} x_{e,2} \end{pmatrix} + \begin{pmatrix} 0 \\ \frac{1}{M} \end{pmatrix} \phi\left(\mathbf{X}_e\right) \right] \\
&= \begin{pmatrix} x_{e,1} & , & x_{e,2} \end{pmatrix} \begin{pmatrix} x_{e,2} \\ \frac{1}{M}\left(-x_{e,2} + \phi\left(\mathbf{X}_e\right)\right) \end{pmatrix} \\
&= x_{e,1} x_{e,2} + \frac{1}{M}\left(-\mu_v x_{e,2}^2 + x_{e,2}\phi\left(\mathbf{X}_e\right)\right).
\end{aligned}$$

In order to stabilize the subsystem we choose $\phi\left(\mathbf{X}_e\right)$, such that

$$\phi\left(\mathbf{X}_e\right) = -M x_{e,1} - k_1 x_{e,2}, \quad k_1 > 0. \tag{3.30}$$

Substituting $\phi\left(\mathbf{X}_e\right)$ into $\dot{V}\left(\mathbf{X}_e\right)$ leads to

$$\dot{V} = -x_{e,2}^2 \frac{\mu_v + k_1}{M}. \tag{3.31}$$

Although $\dot{V}\left(\mathbf{X}_e\right) \leq 0$, the resulting Lyapunov function (3.31) is dependent only on $x_{e,2}$, which means that $\dot{V}$ can be zero regardless of $x_{e,1}$. Therefore we say that $\dot{V}\left(\mathbf{X}_e\right)$ is negative semi-definite and thus it fails to satisfy the asymptotic stability condition (3.29). Nevertheless, according to LaSalle's invariance principle, if we can establish that no trajectory can stay identically at a point where $\dot{V}\left(\mathbf{X}\right) = 0$, except at the origin, then we can say that the origin is asymptotically stable [8].

Following the foregoing argument, we notice that $\dot{V}\left(\mathbf{X}_e\right)$ is negative everywhere, except on the line $x_{e,2} = 0$, where $\dot{V}\left(x_{e,2} = 0\right) = 0$. The subsystem can maintain the condition $\dot{V}\left(\mathbf{X}_e\right) = 0$ only on the line $x_{e,2} = 0$. But,

$$\begin{aligned}
x_{e,2} &\equiv 0 \Rightarrow \dot{x}_{e,2} \equiv 0 \\
&\Rightarrow \zeta_e \equiv 0 \\
&\Rightarrow \left(\frac{m_1}{x_1} - \frac{m_2}{l - x_1}\right) - \left(\frac{m_1}{x_d} - \frac{m_2}{l - x_d}\right) \equiv 0.
\end{aligned}$$

Notice that the last equivalency is possible only when $x_1 = x_d$. Recalling

(3.20), when $x_1 = x_d$ then $x_{e,1} = 0$, which means that the last equivalency is possible only at the origin $(x_{e,1}, x_{e,2}) = (0, 0)$. Hence, the subsystem can maintain the condition $\dot{V}(\mathbf{X}_e) = 0$ only at the origin $\mathbf{X}_e = \mathbf{0}$. Therefore, $V(\mathbf{X}_e(t))$ must decrease toward 0, and $\mathbf{X}_e(t) \to \mathbf{0}$ as $t \to \infty$, which guarantees that the origin is asymptotically stable.

3.5. Backstepping

Adding and subtracting $g(\mathbf{X}_e)\phi(\mathbf{X}_e)$ on the right-hand side of (3.26), we obtain the equivalent representation

$$\dot{\mathbf{X}}_e = [f(\mathbf{X}_e) + g(\mathbf{X}_e)\phi(\mathbf{X}_e)] + g(\mathbf{X}_e)(\zeta_e - \phi(\mathbf{X}_e)) \tag{3.32}$$

$$\dot{\zeta}_e = u, \tag{3.33}$$

which is shown in Figure 3.3.

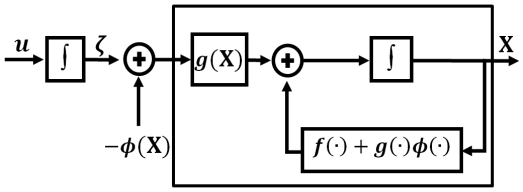

Figure 3.3.: The block diagram of system 3.32-3.33

The change of variables

$$z = \zeta_e - \phi(\mathbf{X}_e) \tag{3.34}$$

results in the system

$$\dot{\mathbf{X}}_e = [f(\mathbf{X}_e) + g(\mathbf{X}_e)\phi(\mathbf{X}_e)] + g(\mathbf{X}_e)z \tag{3.35}$$

$$\dot{z} = u - \dot{\phi}. \tag{3.36}$$

The transition from the system (3.32)-(3.33) to the system (3.35)-(3.36), which is shown in Figure 3.4, can be viewed as "backstepping" $-\phi(\mathbf{X}_e)$ through the integrator.

We obtain $\dot{\phi}$ by

$$\dot{\phi} = \frac{\partial \phi}{\partial \mathbf{X}_e} \left[f\left(\mathbf{X}_e\right) + g\left(\mathbf{X}_e\right) \zeta_e \right].$$

Having f, g, and ϕ already defined,

$$\begin{aligned} \dot{\phi} &= \left(\frac{\partial \phi}{\partial x_{e,1}}, \frac{\partial \phi}{\partial x_{e,2}} \right) \begin{pmatrix} \dot{x}_{e,1} \\ \dot{x}_{e,2} \end{pmatrix} \\ &= (-1 - k_1) \begin{pmatrix} x_{e,2} \\ \frac{1}{M} \left(\zeta_e - \mu_v x_{e,2} \right) \end{pmatrix} \\ &= -x_{e,2} - \frac{k_1}{M} \left(\zeta_e - \mu_v x_{e,2} \right). \end{aligned} \tag{3.37}$$

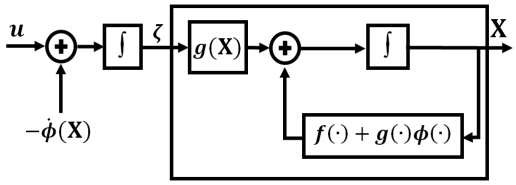

Figure 3.4.: The block diagram of system 3.35-3.36

3.6. Stability of the Overall System

We now show how to stabilize the overall system. By taking $\nu = u - \dot{\phi}$ we reduce the system (3.35)-(3.36) to the cascade connection

$$\begin{aligned} \dot{\mathbf{X}}_e &= \left[f\left(\mathbf{X}_e\right) + g\left(\mathbf{X}_e\right) \phi\left(\mathbf{X}_e\right) \right] + g\left(\mathbf{X}_e\right) z \\ \dot{z} &= \nu, \end{aligned}$$

which is similar to the system we started from (i.e., system 3.26-3.27), except that now the first component has an asymptotically stable origin when the input is zero. This feature is exploited in the design of ν to stabilize the overall system. Using

$$V_o\left(\mathbf{X}_e, z\right) = V\left(\mathbf{X}_e\right) + \frac{1}{2} z^2$$

as a Lyapunov function, we obtain

$$\begin{aligned}\dot{V}_o &= \frac{\partial V}{\partial \mathbf{X}_e}\left[f\left(\mathbf{X_e}\right)+g\left(\mathbf{X}_e\right)\phi\left(\mathbf{X}_e\right)\right]+\frac{\partial V}{\partial \mathbf{X}_e}g\left(\mathbf{X}_e\right)z+z\dot{z}\\ &= \dot{V}\left(\mathbf{X}_e\right)+\frac{\partial V}{\partial \mathbf{X}_e}g\left(\mathbf{X}_e\right)z+z\nu.\end{aligned}$$

Choosing

$$\nu=-\frac{\partial V}{\partial \mathbf{X}_e}g\left(\mathbf{X}_e\right)-k_2 z,\quad k_2>0 \tag{3.38}$$

yields

$$\dot{V}_o=\dot{V}\left(\mathbf{X}_e\right)-k_2 z^2,$$

which shows that $\dot{V}_o \leq 0$. If $z=0$ then the system is located exactly where the subsystem is. We have already shown that $\dot{V}$ guarantees asymptotic stability at $\mathbf{X}_e=\mathbf{0}$. Therefore, the origin $(\mathbf{X}_e, z)=(\mathbf{0},0)$ is asymptotically stable. Since $\phi\left(\mathbf{0}\right)=0$, we conclude that the origin $(\mathbf{X}_e,\zeta_e)=(\mathbf{0},0)$ is also asymptotically stable. Finally, we can calculate the state feedback control law

$$u=\dot{\phi}+\nu. \tag{3.39}$$

Since $\dot{\phi}$ is already derived, we are left to calculate ν. Using (3.38) we have

$$\begin{aligned}\nu &= -\begin{pmatrix}\frac{\partial V}{\partial x_{e,1}} & \frac{\partial V}{\partial x_{e,2}}\end{pmatrix}\begin{pmatrix}0\\1\end{pmatrix}-k_2\left(\zeta_e-\phi\left(\mathbf{X}_e\right)\right)\\ &= -x_{e,2}-k_2\left(\zeta_e+Mx_{e,1}+k_1x_{e,2}\right).\end{aligned} \tag{3.40}$$

Substituting (3.37) and (3.40) into 3.39, we obtain

$$u = -2x_{e,2}-\frac{k_1}{M}\left(\zeta_e-\mu_v x_{e,2}\right)-k_2\left(\zeta_e+Mx_{e,1}+k_1x_{e,2}\right).$$

The consequential state feedback control law is a function of $x_{e,1}$, $x_{e,2}$ and ζ_e, which is, in itself, a function of m_1 and m_2; $x_{e,1}$ is acquired by the real-time measurement of x_1, and the reference signal x_d; $x_{e,2}$ is acquired by the the time derivative of x_1 (i.e. x_2), and $\dot{x}_d$ is the time derivative of the reference signal; m_1 and m_2 are calculated by the ideal gas law (2.6) using the real-

time measured pressures. The controller gains were set in simulation such that the input cannot exceed the valve's input limitations; therefore, in our experiments we set $k_1 = k_2 = 5$.

4. Simulation and Experiments

This chapter introduces and discusses the simulation and the experiment's results of the pneumatic system under scope. In Section 4.1 we validate the dynamic model derived in Chapter 2 by comparing its simulation with measurements from the real actuator, which is integrated into the test rig (see Appendix C). Then, in Section 4.2 the control performance is evaluated for position tracking. The control experiments are conducted using two configurations: First the actuator is free of external force, and after it is subjected to a resisting mechanical spring which emulates an external force with a varying magnitude, as illustrated in Figure 4.1.

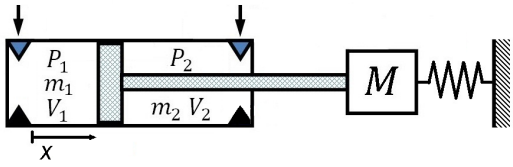

Figure 4.1.: The test rig scheme as configured in the control tests: The pneumatic actuator is connected to an external load M, to increase the self mass, and to a spring that emulates the varying external force

4.1. Actuator's Dynamic Model Validation

The backstepping control law, introduced in Chapter 3, is derived based on the dynamical model of the controlled system. In this thesis we propose an original approach to the derivation of the actuator's dynamical model (see Chapter 2). Therefore, it is necessary to verify the accuracy of the model by simulation and experimentation of the actuator response.

The simulation code is represented by the block diagram of the Simulink software, as shown in Figure 4.2. Its purpose is to forecast the actuator position given the initial position, initial velocity, and initial masses of air in the actuator's chambers.

The air mass is directly computed by the ideal gas law (2.6), using the measured pressures and position. Then the velocity and the acceleration are computed using the state space of the model's equation of motion, i.e., by (2.16). The simulated position is computed by integration of the velocity with respect to the time.

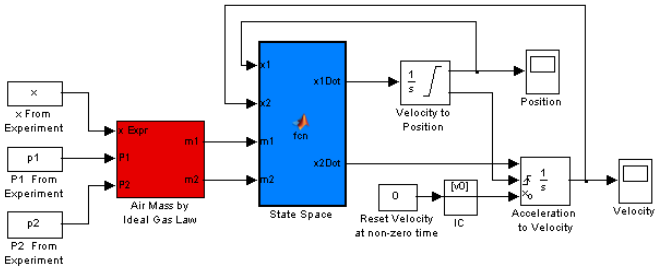

Figure 4.2.: The simulation code in the Simulink software

A comparison of the simulated actuator response with the experiment results is shown in Figure 4.3 (a) and the error is shown in Figure 4.3 (b). The displacement of the actuator is a reaction to the valve input shown in Figure 4.3 (c). In the validation test the actuator is free of external force (the spring is not integrated in this test). The small simulation error, in the bounds of ± 0.006[m], indicates that the dynamical model is sufficiently accurate. Possible reasons for the error are:

1. Although we used data provided by the manufacturer, we found inaccurate geometric measures, such as that of the dead-volume.

2. The friction model includes only viscous friction effects and does not include static friction, hysteresis, or stick-slip phenomena.

3. The model does not count transition effects of the air inside the actuator.

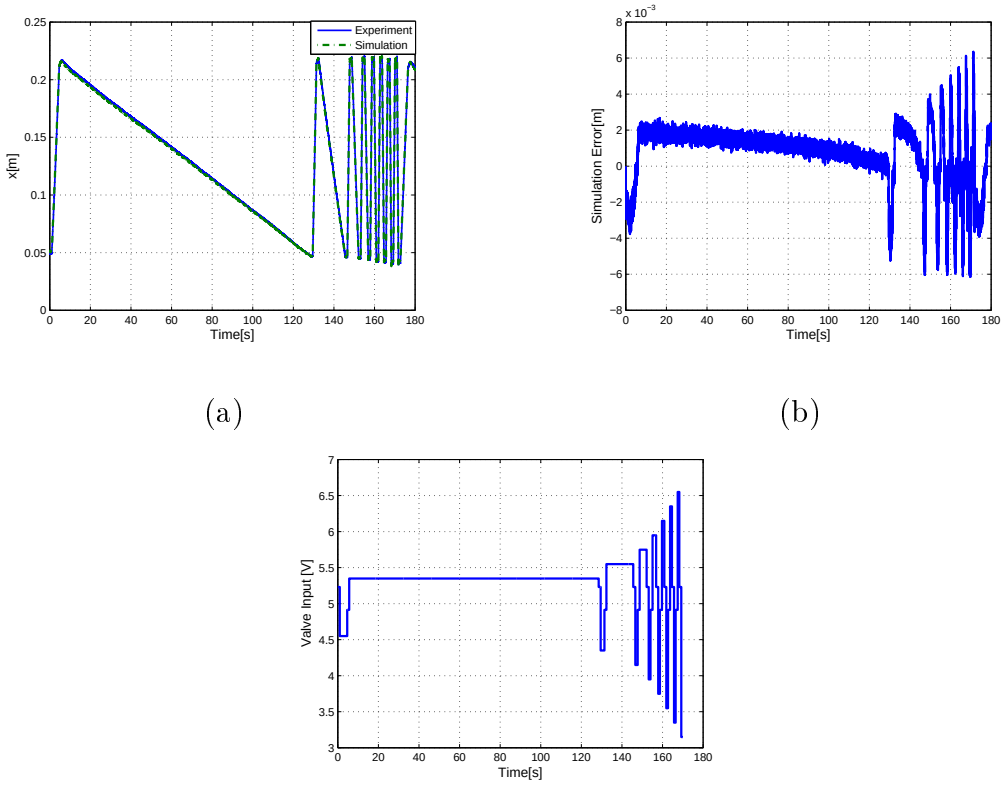

Figure 4.3.: Validation results: (a) the simulation and the experiment plots, (b) the simulation error, and (c) the valve input

4.2. Control Performance

The stability of the system under scope is mathematically proven in Chapter 3, but it was important to show that the control strategy could apply to a real pneumatic system, knowing the difficulties that arise from the nature of its physics. This subsection analyzes experimental results of the control performance as implemented on the test rig (described in Appendix C).

We present here results of tests in which the actuator's position tracks a position reference trajectory signal of a square wave and a sinusoidal wave. To imitate a real working environment, such as when the actuator is integrated into the legs of a walking robot, we added a mechanical spring that emulates a

varying external force. The spring is integrated into the test rig, as illustrated in Figure 4.1. We should mention that the external force generated by the spring is considered to be an unknown disruption. It is not directly measured by a force gauge and is only evaluated offline for analysis.

We start with the test results of tracking a square wave trajectory. The square wave is a combination of two states; the upper step where $x_d = 0.2$[m], and the lower step where $x_d = 0.1$[m]. Figure 4.4 (a) and Figure 4.5 (a) show the position response of the actuator, when it is free of external force and when it is subjected to the force exerted by the spring, respectively. We notice that with the aid of the spring the error in the lower step is eliminated, though the upper step is not fully reached, leaving a minimum error of 0.005[m]. Without the spring, the minimum error of the lower step is 0.003[m] and there is zero error in the upper step. We refer to these errors as steady state errors. Inspection of the the valve input as seen in Figures 4.4 (b) and 4.5 (b) reveals that although appropriate input is received, the steady state error remains. We conclude that this behavior is due to poor operation of the valve in the neighborhood of 5[v] (for more information on the valve's behavior characteristics, see Appendix D). Another phenomenon we notice in both tests is a short retreat during the transient response, which is also evident in the valve input figures. Future work will include the study of the cause of this phenomenon and how to avoid it. The evaluated external force exerted by the spring, shown in Figure 4.5 (c), varies from 250[N] to 950[N].

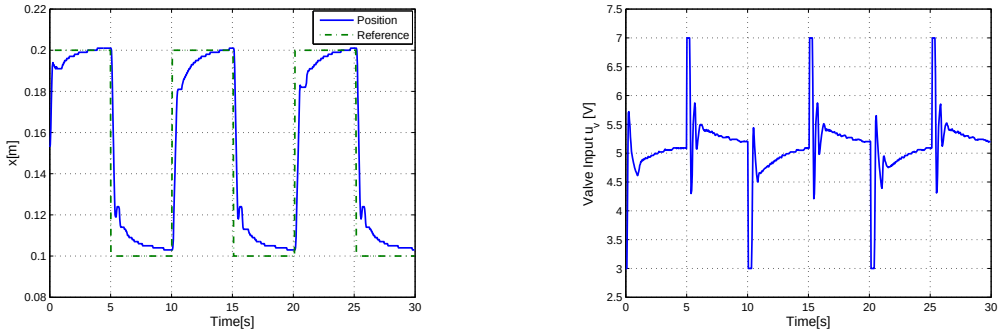

(a) (b)

Figure 4.4.: Tracking square wave reference when the actuator is free of external force: (a) real position and the position reference, and (b) the valve input

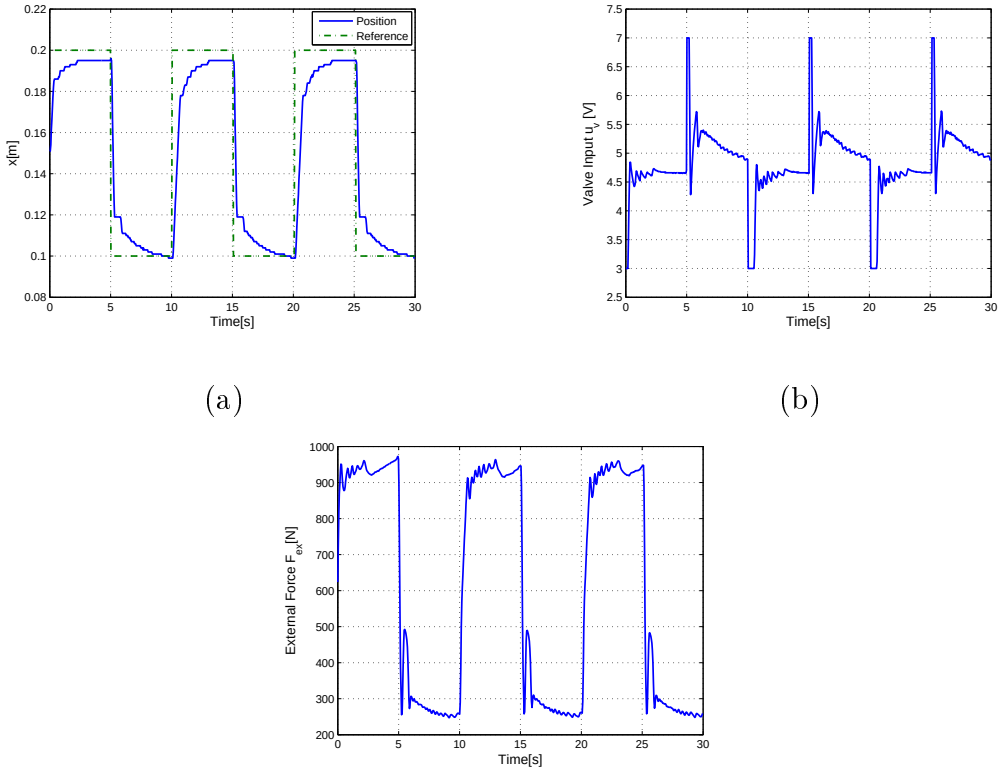

Figure 4.5.: Tracking square wave reference with spring emulating external force: (a) real position and the reference position, (b) the valve input, and (c) the external force applied to the actuator by the spring

We continue and analyze the tests results of tracking a sinusoidal wave trajectory. The pich-to-pick amplitude of the reference is 0.12[m] and the frequency is 0.15[Hz]. Figure 4.6 (a) and Figure 4.7 (a) show the position response of the actuator, when it is free of external force and when it is subjected to the force exerted by the spring, respectively. The tracking error is within the bounds of ± 0.01[m] in both tests, as shown in Figures 4.6 (b) and 4.7 (b). The magnitude of the external force varies from 250[N] to about 1050[N], as seen in Figure 4.7 (d). This force constitutes a significant disturbance to the actuator, considering it can produce a maximum force of about 1600[N] in the given configuration. In contrast to the square wave tracking,

here the addition of the external force is hardly noticed, but we do get a somewhat fragmented motion. The explanation for this last behavior is the proximity of the valve input to 5[v], as seen in Figures 4.6 (c) and 4.7 (c); there is a dead-band from 4.7 to 5.3[v], which results in poor response of the valve. During the controlled motion, the tracking error decreases and the valve input tends to 5[v], where flow through it is halted. With time, the tracking error increases and the valve input exits the dead-band and resumes motion.

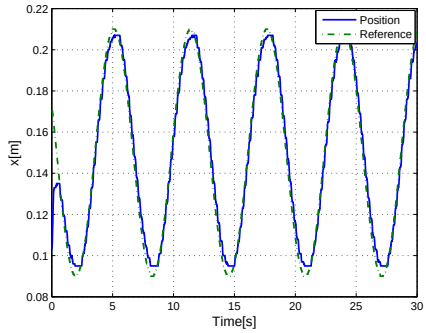

(a)

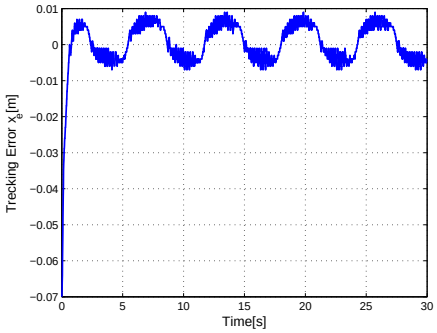

(b)

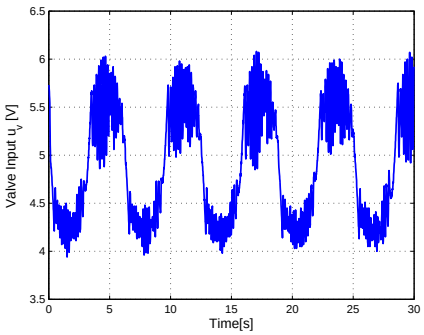

(c)

Figure 4.6.: Tracking sinusoid reference without external force: (a) real position and the reference position, (b) the tracking error, and (c) the valve input

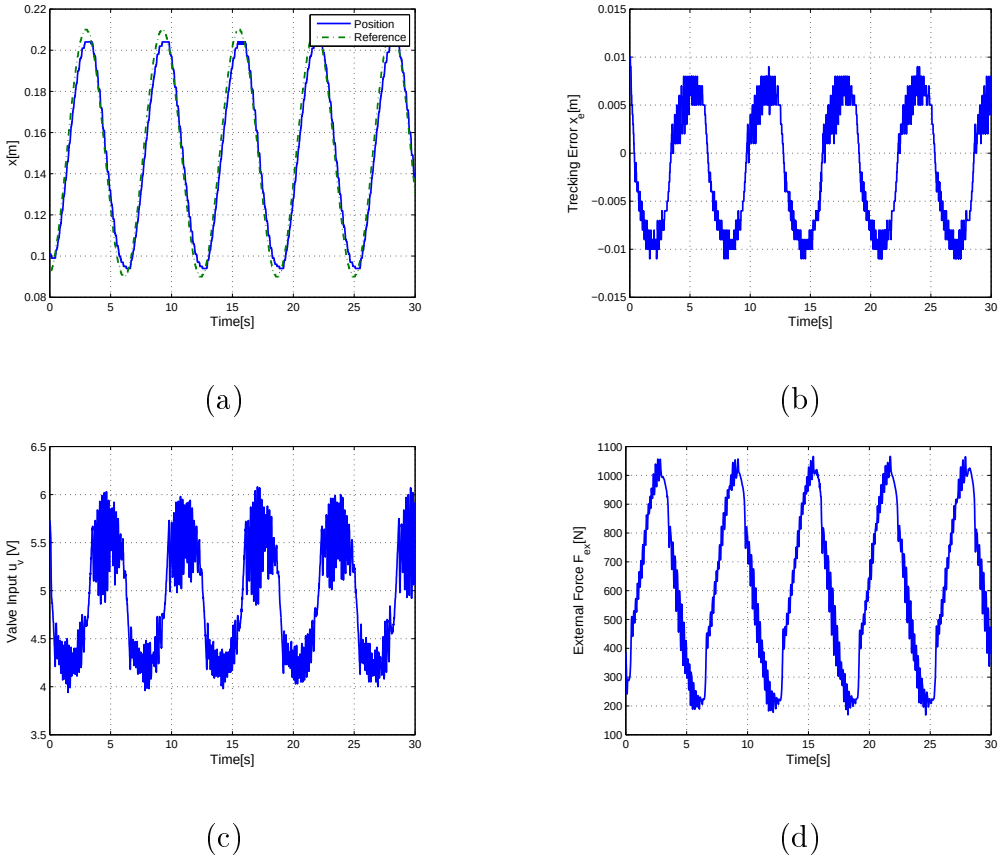

Figure 4.7.: Tracking sinusoid reference with spring emulating external force: (a) real position and the position reference, (b) the tracking error, (c) the valve input, and (d) the external force applied to the actuator by the spring

5. Summary

This thesis deals with the development of a position control of a pneumatic actuation system, which is subjected to a disturbance of a time varying external force. In addition to the main goal of implementing a controller to satisfy control demands, we have achieved two additional developments in this work, which we will summarize here.

In Chapter 2 we introduced an original modeling method of the pneumatic actuator. While previous papers traditionally use the Newton second law to model the actuator, we utilized energy principles to derive a multidomain Lagrangian of the actuator. It is composed of mechanical kinetic energy and pneumatic potential energy, and is the basis for the equation of motion. The validation of this model, included in section 4.1, exhibits a relatively small error in the bounds of ± 0.006[m].

Utilizing the actuator's model, in Chapter 3 we applied the nonlinear backstepping method, to derive a state feedback control law. We used the derivative of the potential energy to define the tracking error. The experiment's results, provided in Chapter 4, prove that the controller is able to track a position reference trajectory while the actuator is subjected to a external force, which varies from 250[N] to 1050[N]. Actually, the effect of the addition of the external force on the performance was minor.

A. Thermodynamic Processes

A.1. Isothermal Process

An isothermal process is when a thermodynamic system changes but the temperature remains constant, i.e., $\Delta T = 0$ but $Q \neq 0$ (ΔT is the temperature difference and Q is the heat transfer). An isothermal process obeys the relation:

$$PV = Constant,$$

where P is the pressure and V is volume.

A.2. Polytropic Process

A polytropic process is a thermodynamic process that is reversible and obeys the relation:

$$PV^n = Constant,$$

where n, the polytropic index, is any real number. This equation can be used to accurately characterize processes of certain systems, notably the compression or expansion of a gas.

A.3. Adiabatic Process

An adiabatic process is any process occurring without gain or loss of heat within a system; that is, during the process the system is thermodynamically isolated, meaning there is no heat transfer with the surroundings. In an adiabatic process, $\Delta T \neq 0$ but $Q = 0$. The mathematical equation for an

ideal gas undergoing a reversible adiabatic process is

$$PV^{\gamma} = Constant,$$

where $\gamma = 1.4$ for air.

B. Mathematical Definitions

B.1. Strict-Feedback Form

In control theory, dynamical systems are in strict-feedback form when they can be expressed as

$$\begin{cases} \dot{\mathbf{x}} = f_0(\mathbf{x}) + g_0(\mathbf{x})z_1 \\ \dot{z}_1 = f_1(\mathbf{x}, z_1) + g_1(\mathbf{x}, z_1)z_2 \\ \dot{z}_2 = f_2(\mathbf{x}, z_1, z_2) + g_2(\mathbf{x}, z_1, z_2)z_3 \\ \vdots \\ \dot{z}_i = f_i(\mathbf{x}, z_1, z_2, \ldots, z_{i-1}, z_i) + g_i(\mathbf{x}, z_1, z_2, \ldots, z_{i-1}, z_i)z_{i+1} \quad \text{for } 1 \leq i < k-1 \\ \vdots \\ \dot{z}_{k-1} = f_{k-1}(\mathbf{x}, z_1, z_2, \ldots, z_{k-1}) + g_{k-1}(\mathbf{x}, z_1, z_2, \ldots, z_{k-1})z_k \\ \dot{z}_k = f_k(\mathbf{x}, z_1, z_2, \ldots, z_{k-1}, z_k) + g_k(\mathbf{x}, z_1, z_2, \ldots, z_{k-1}, z_k)u \end{cases}$$

where $\mathbf{x} \in \mathbb{R}^n$ with $n \geq 1$, $z_1, z_2, \ldots, z_i, \ldots, z_{k-1}, z_k$ are scalars, u is a scalar input to the system, $f_0, f_1, f_2, \ldots, f_i, \ldots, f_{k-1}, f_k$ vanish at the origin (i.e., $f_i(0, 0, \ldots, 0) = 0$), and $g_1, g_2, \ldots, g_i, \ldots, g_{k-1}, g_k$ are nonzero over the domain of interest (i.e., $g_i(\mathbf{x}, z_1, \ldots, z_k) \neq 0$ for $1 \leq i \leq k$). Here, strict feedback refers to the fact that the nonlinear functions f_i and g_i in the $\dot{z}_i$ equation only depend on states $x, z_1, \ldots, z_i$ that are fed back to that subsystem. That is, the system has a kind of lower triangular form. [8]

B.2. Stability and Asymptotic Stability

Consider the autonomous system

$$\dot{x} = f(x), \tag{B.1}$$

where $f : D \to R^n$ is a local Lipschitz from a domain $D \subset R^n$ into R^n. Suppose $\bar{x} \in D$ is an equilibrium point of B.1; that is, $f(\bar{x}) = 0$. Our goal is to characterize and study the stability of $\bar{x}$. For convenience, the equilibrium point is at the origin of R^n; that is, $\bar{x} = 0$.

Definition. *The equilibrium point $x = 0$ of B.1 is*

- *stable if, for each $\epsilon > 0$, there is $\delta = \delta(\epsilon) > 0$ such that*

$$\|x(0)\| < \delta \Rightarrow \|x(t)\| < \epsilon, \qquad \forall t \geq 0$$

- *unstable if it is not stable*
- *asymptotically stable if it is stable and δ can be chosen such that*

$$\|x(0)\| < \delta \Rightarrow \lim_{t \to \infty} x(t) = 0.$$

[8]

B.3. Lyapunov Stability Theorem

Theorem. *Let $x = 0$ be an equilibrium point for B.1 and $D \subset R^n$ be a domain containing $x = 0$. Let $V : D \to R^n$ be a continuously differentiable function such that*

$$V(0) = 0 \text{ and } V(x) > 0 \text{ in } D - \{0\}$$

$$\dot{V}(x) \leq 0 \text{ in } D.$$

Then, $x = 0$ is stable. Moreover, if

$$\dot{V}(x) < 0 \text{ in } D - \{0\}$$

then $x = 0$ is asymptotically stable. [8]

B.4. Positive Definite

Definition. *A real-valued, continuously differentiable function f is positive definite on a neighborhood of the origin, D, if $f(0) = 0$ and $f(x) > 0$ for every non-zero $x \in D$.* [14]

C. Test Rig

This appendix describes the test rig, as seen in Figure C.1, that we specially built in order to validate the dynamical model derived in Chapter 2 and to test the control solution of Chapter 3.

The test rig includes all the components needed for controlled actuation: (1) a BACCARA S3000 pneumatic actuator with a cylinder of a 0.063[m] diameter bore, a 0.02[m] diameter rod and a 0.3[m] stroke, (2) a 5/3 proportional directional control valve of the Festo MPYE series, (3) a Celesco SP1 potentiometer (not shown) for position measurement, (4) two SMC ISE30 series pressure gauges, and (5) an electronic circuit for control and data acquisition. To emulate a real working environment, we added: (6) a horizontal rail, (7) a slider on which the (8) external load is connected, and (9) a spring that generates a varying external force.

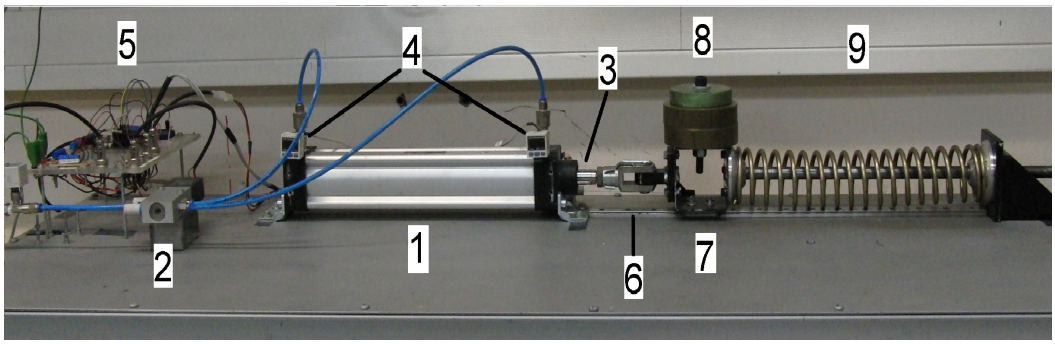

Figure C.1.: Test rig

The electronic circuit, seen in Figure C.2, includes: (1) a ARDUINO UNO micro-controller to acquire data from the system and calculate the controller

input, (2) a Microchip 12bit digital to analog converter that converts digital input from the micro controller to an analog signal, (3) an amplifier that is configured to span the analog signal to the input range of the valve, (4) input and output data ports and (5) power supply connectors.

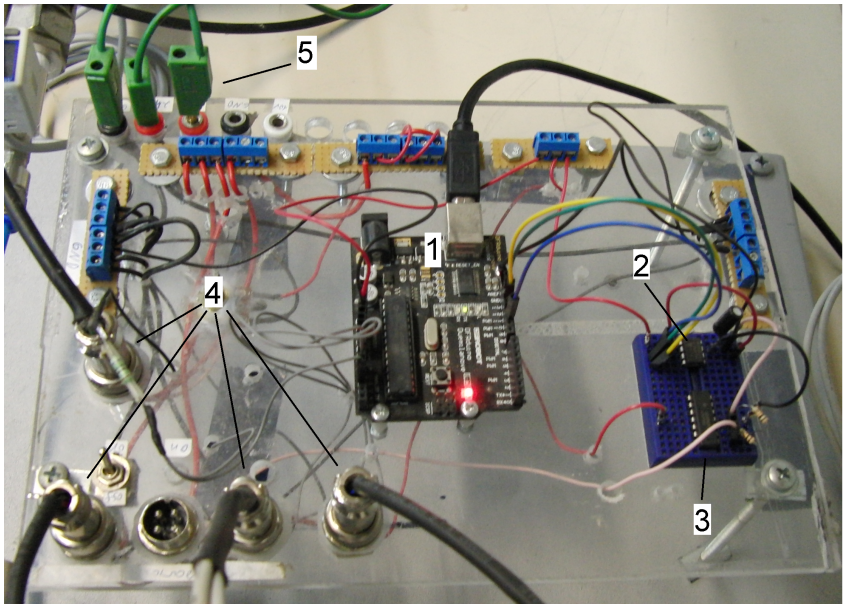

Figure C.2.: Test rig

D. The Mass Flow-Rate Model

The pneumatic valve is the control element of the pneumatic system. It controls the flow of air into and out-of the actuator. Thus, it changes the mass of air in the chambers of the actuator, which leads to pressure change and therefore causes movement. In this appendix we introduce an original method that we developed to model the mass flow-rate of air which passes through the valve[1].

This appendix is arranged as follows: We start, in Section D.1, with a detailed description of the pneumatic valve used in this project - the proportional directional control valve. The next section, Section D.2, provides a review on modeling of the mass flow-rate of a compressible gas. We introduce the two common models that can be found in the literature: the analytical model and the engineering model. The latter is an approximation of the first. In both models the flow-rate is a function of the pressure ratio, which is the downstream pressure divided by the upstream pressure.

By comparing these models with real measurements in Section D.3, we discovered that the behavior of the flow-rate through the valve under scope does not agree with the theory. Therefore, we developed a method of modeling, which is based on system identification, by which the flow-rate is a function of the pressure ratio and the valve input. This method, described in Section D.4, separates the identification process into two parts: Section D.5 suggests a method to fit a function that describes the behavior of the flow with respect to the input, and Section D.6 deals with the flow function, which represents

[1] This appendix describes complementary work done to accurately model the flow-rate through the control valve. Although for control purposes a simplified flow-rate model is used, significant work had been done to develop an innovative modeling method with an outcome of a model with a very good fit. Therefore, we decided to include it in the thesis as an appendix.

the dependency of the flow-rate on the pressure ratio. Finally, in Section D.7 we integrate the two partial models into a complete three dimensional model of the mass flow-rate as a function of the input and the pressure ratio.

D.1. Proportional Directional Control Valve

Figure D.1.: Festo MPYE-5 proportional directional control valve and its schematic symbol

This section deals with a specific type of valve which was chosen for this project - the 5/3 proportional directional control valve, shown in Figure D.1. The valve is manufactured by Festo and the model mark is MPYE-5-1/8 HF-010B. The schematic symbol, on the right side of Figure D.1, indicates that the valve consists of five ports. It is directly actuated by a position-controlled spool, which transforms an analog input signal into a corresponding opening cross-section at the valve outputs. The valve input signal range is between 0[v] to 10[v], and according to the official manual [15] the valve mid position is at 5 ± 0.1[v], the maximum flow-rate[2] is 700[l/min], the bandpass limit ("critical frequency") is at 100[Hz], and the power supply is 17-30[v].

The valve is connected to other components of the a pneumatic system, such that: port 1, the supply port, is connected to a reservoir of high pressurized air at 6[bar] to 10[bar], port 2 and port 4 are connected to the actuator's ports and port 3 and port 5 are the exits to the atmosphere.

[2]Based on standard conditions set by Festo: ambient temperature - 20^0[C], ambient pressure - 1.013[bar], supply pressure - 6[bar] and exit pressure - 5[bar].

The operational logic of the valve is as follows: When the input range is from 0[v] to 5[v], a passage will open to allow inlet flow to the actuator from port 1 to port 2 and outlet flow from the actuator at port 4 to the atmosphere at port 5. When the input range is from 5[v] to 10[v], a passage will open to allow inlet flow to the actuator from port 1 to port 4 and outlet flow from the actuator at port 2 to the atmosphere at port 3.

A qualitative and general diagram of the flow-rate through the valve is shown in Figure D.2. This figure, which is taken from the manual, describes the volumetric flow-rate, in percentage, as a function of the input in volts. Careful examination of this figure brings out the following issues:

1. The diagram is not aimed specifically to the valve under scope, rather it represents a generalized flow for all the valves in the series MPYE-5. These valves differ in geometry in order to allow different flow-rate ranges from 100[l/min] to 2000[l/min]. Therefore, we must expect inaccuracy in an unknown ratio.

2. There is no record of the way the flow is influenced by the pressures in the ports. The diagram shows a static condition where the upstream pressure is at 6[bar] and the downstream pressure is at 5[bar]. There is no information on the behavior in other situations.

3. The curve implies that the flow is almost a linear function of the input from both sides of the middle, i.e., 5[v]. Test results reveal a different behavior - clearly non-linear by which a major change in the flow-rate takes place when the input ranges from 3[v] to 7[v], while in the rest of the range, the change is minor.

4. The diagram shows no indication of leakage, although the manufacturer acknowledges that it exists and states a maximum of 25[l/min] for the relevant valve. According to Festo this leakage is measured in new conditions with a supply pressure of 6[bar] and when all other ports are closed.

5. The diagram displays a kind of "dead-band" in the area around 5[v].

Test results indicate a poor response at the input range of 4.7[v] to 5.2[v].

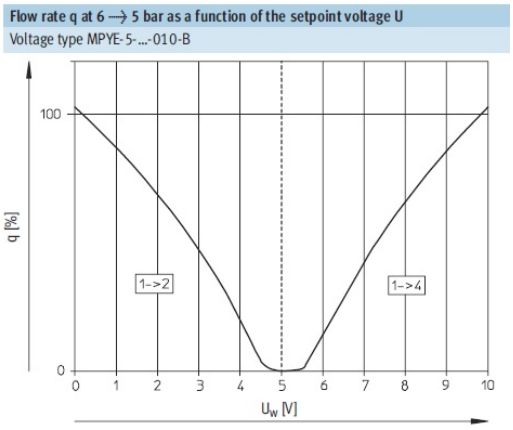

Figure D.2.: Flow-rate as a function of the valve input - manufacturer's manual

D.2. Background on Compressible Flow-Rate

D.2.1. Analytical Model

Tracing the origins of the scientific research on pneumatics, we find that the first complete model of compressible flow through a restriction was given by St. Venant and Wantzel in 1839 [1]. This model is based on a system of a huge reservoir from which air is discharged through a well-rounded nozzle into the atmosphere, as depicted in Figure D.3. Five assumptions are taken in order to derive the model:

- The nozzle has a specific geometric structure, by which the curvature is well-rounded and the diameter equals the length. It allows no flow contraction.
- A huge reservoir allowing pressure P_1, mass m_1, and temperature T_1 to be considered as constants.
- The approach velocity of the air is negligible.

- The process is adiabatic, i.e., there is no heat exchange while air passes through the nozzle.
- The nozzle's cross section is rounded.

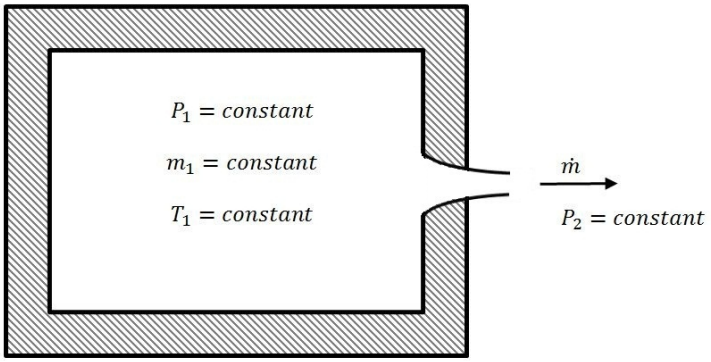

Figure D.3.: Huge reservoir with a nozzle

Modern control valves are not designed with a well rounded nozzle, rather a sharp edge orifice is used to control the flow-rate. A sharp edge orifice is less flow effective than the nozzle, since it enhances more resistance to air flow. To extend the analysis to the flow through a sharp edged orifice, the discharge coefficient C_d is introduced. The model's equation is therefore

$$\dot{m} = AC_d P_1 \sqrt{\frac{2}{RT_1}} \psi \,, \tag{D.1}$$

where A is the cross section of the orifice and ψ is the flow-rate piecewise function, as illustrated in Figure D.4. The flow function is dependent on the pressure ratio, P_r, which is the division of the downstream pressure, P_d, by the upstream pressure, P_u, i.e.,

$$P_r = \frac{P_d}{P_u}. \tag{D.2}$$

When pressure ratio is greater than the critical pressure ratio, P_{cr}, sub-sonic flow takes place and flow depends non-linearly on both upstream and downstream pressures. When pressure ratio is smaller or equal to the critical

pressure ratio, then flow is in choked mode. In the later case, flow depends linearly solely on the upstream pressure. The flow function is defined by

$$\psi = \sqrt{\frac{\gamma}{\gamma-1}} \begin{cases} \left(\frac{2}{\gamma+1}\right)^{1/(\gamma-1)} & , P_r \leq P_{cr} \\ \sqrt{P_r^{2/\gamma} - P_r^{(\gamma+1)/\gamma}} & , P_r > P_{cr} \end{cases} , \tag{D.3}$$

where $\gamma = {}^{C_p}/_{C_v} = 1.4$ is the specific heat capacity ratio of air. Using the value of γ, we can calculate the critical pressure ratio

$$P_{cr} = \left(\frac{2}{\gamma+1}\right)^{\frac{\gamma}{\gamma-1}} = 0.528\,.$$

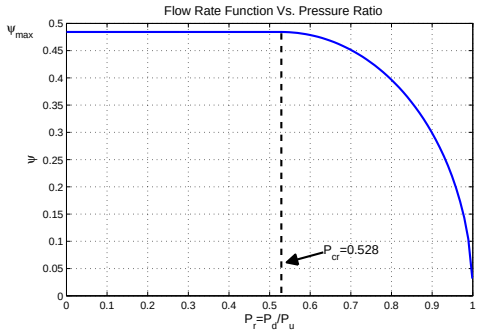

Figure D.4.: The flow function $\psi\,(P_r)$

D.2.2. Engineering Approximation of the Mass Flow-Rate

Calculation of the mass flow-rate by the analytical model was not a simple manner before the modern PC emerged in the 1980s. The value of the discharge coefficient, C_d, and the orifice cross section, A, had to be identified through experiments (usually manufacturers did not provide details about them). Moreover, when dealing with varying cross section valves, such as the proportional directional valve, the C_d also varies. In order to acquire a suitable model of the flow, the dependency of these two parameters on the input had to be identified.

The difficulty in identifying A and C_d, and the relative complexity of the model's equations, (D.1) and (D.3), encouraged Sanville in 1971 to propose an approximation to the analytic model, which later became the basis for the standard ISO 6358[3] [1]. The approximation model is

$$\dot{m} = P_1 C \rho_0 \sqrt{\frac{T_0}{T_1}} \begin{cases} 1 & , \ P_r \leq b \\ \sqrt{1 - \left(\frac{P_r - b}{1 - b}\right)^2} & , \ P_r > b \end{cases}, \tag{D.4}$$

where C is the sonic conductance, b is the critical pressure ratio (referred to earlier as P_{cr}), and ρ_0 and T_o are the density and the temperature of air at reference conditions. The sonic conductance, C, equals the mass flow-rate through the component, $\dot{m}_{choked}$, divided by the product of upstream pressure, P_1, and the mass density at standard conditions, ρ_0, when the flow is choked. That is,

$$C = \frac{\dot{m}_{choked}}{P_1 \rho_0}. \tag{D.5}$$

Substituting (D.5) into (D.4) results in

$$\dot{m} = \dot{m}_{choked} \sqrt{\frac{T_0}{T_1}} \begin{cases} 1 & , \ P_r \leq b \\ \sqrt{1 - \left(\frac{P_r - b}{1 - b}\right)^2} & , \ P_r > b \end{cases}. \tag{D.6}$$

In order to use the approximation model we must identify the two describing parameters, C and b. The ISO 6358 standard details the experimental setup and procedure for identifying these parameters.

D.3. Experiment Results

In this section we provide results and conclusions from the valve test that was conducted according to the ISO 6358 standard. The test procedure involved measurement of the volumetric flow-rate and the upstream and downstream

[3]The international standard ISO 6358, published in 1989, specifies a method for testing pneumatic fluid power components which use compressible fluids, i.e., gases, to enable their flow-rate characteristics under steady-state conditions[16].

pressures, for different resistances to flow. A change in the resistance to flow, done with another valve, produced a change in the flow-rate and in the downstream pressure. To test the influence of the input on the flow-rate, we conducted a series of the described procedures for various inputs.

We examine Figure D.5, which shows the results from the valve experiment. For clarity, the figure includes only seven data sets arbitrarily chosen out of a larger database that was recorded. The vertical axis represents the measured volumetric flow-rate, q, which is plotted against the measured pressure ratio, P_r. Each data set was measured while the valve input was constant, thus it has a different flow-rate span.

Note: We demonstrate the identification process only for port 4. In order to have a complete model of the valve, the process should be repeated for ports 2, 3, and 5.

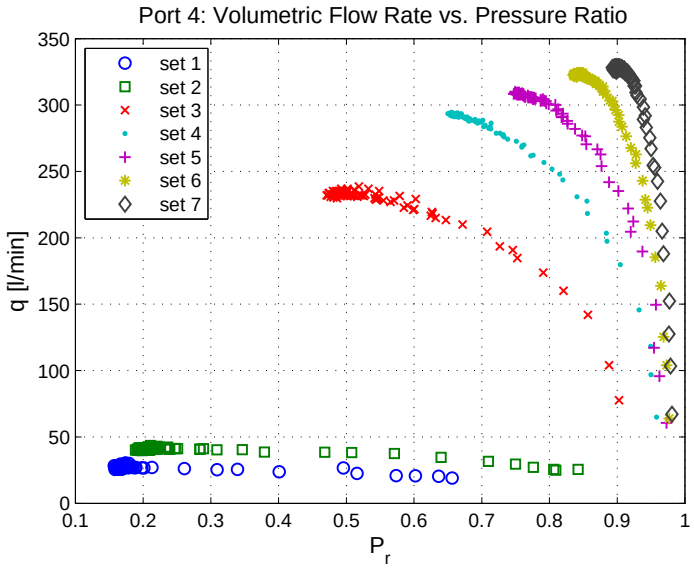

Figure D.5.: Test results: volumetric flow-rate as a function of the pressure ratio for various constant inputs

Analysis of Valve Test

Observing the valve test results, we note four important conclusions:

1. The flow-rate extinguishes as P_r approaches unity. This is an expected behavior that was observed in all data sets.

2. The input increase caused two effects: (a) it increased the span of the flow-rate on the vertical axis, and (b) it narrowed the pressure ratio range.

3. Each data set has an extinguishing behavior with respect to P_r. This behavior resembles the analytic flow function ψ, illustrated in the Figure D.4. Unlike in the theory, the choked flow and the critical pressure ratio are not clearly distinguished in the data sets.

4. Attempting to identify the critical pressure ratio, b, by associating the horizontal location of the point where extinguishing starts, we notice that it changes with each data set. Thus, it cannot have a constant value as in theory. Furthermore, for the majority of the data sets, it seems that b is greater than 0.528 (the theoretical value for a well-rounded nozzle; see Section D.2). The last observation raises a conflict, since, according to Beater [1], the typical value of b is smaller than 0.5, and can be as small as 0 for proportional directional control valves - the type of valve under scope.

The observation that b is not constant and that it is higher than in the theory and reference works, led us to suspect that fitting the theoretical approximation model to the specific valve would be inaccurate. The failure to establish a clear relation between the test results and the theoretical model, and the fact that neither of the two models comprise the reaction to the valve input, motivated us to consider an alternative model.

D.4. Method of Modeling

In this section we propose an alternative model to the mass flow-rate. The modeling process mainly involves experimental identification, such as in the work of Olaby et al. [17] and Rao and Bone [12]. Both of them, for example,

preferred fitting a three dimensional interpolation polynomial over using the theoretical models equation. The approach taken in this thesis is to combine the two concepts; thus, we derive a new empirical model which is based on the theoretical model structure.

Referring to the approximation model which is defined by (D.6),

$$\dot{m} = \underbrace{\dot{m}_{choked}\sqrt{\frac{T_0}{T_1}}}_{f_1} \underbrace{\begin{cases} 1 & , \ P_r \leq b \\ \sqrt{1-\left(\frac{P_r-b}{1-b}\right)^2} & , \ P_r > b \end{cases}}_{f_2}, \tag{D.7}$$

we can consider the mass flow-rate as a product of two components, f_1 and f_2, and write

$$\dot{m} = f_1 f_2.$$

The f_1 and f_2 are functions that we want to identify by using the valve experiment results. The identification process is done separately for each component, based on the assumption that f_1 depends on the valve's input, u, while f_2 depends on the pressure ratio, P_r. Therefore, we define the mass flow-rate such that

$$m\left(\dot{u}, P_r\right) = f_1\left(u\right) f_2\left(P_r\right). \tag{D.8}$$

D.4.1. f_1 - Flow as a Function of the Valve Input u

Before we start to describe how we identify the f_1, we need to explain why it is a function of the input, u. Referring to the engineering approximation model in (D.7), we defined f_1 such that it replaces the expression $\dot{m}_{choked}\sqrt{\frac{T_0}{T_1}}$. We now analyze this expression:

- The maximum mass flow-rate at specific conditions $\dot{m}_{choked}$, varies with the cross section of the valve's orifice. In a proportional directional control valve, the orifice cross section is proportional to the position of the spool, which is the moving part inside the valve. Thus, the spool position determines the maximum mass flow-rate possible, i.e., it determines $\dot{m}_{choked}$. Neglecting the spool dynamics[4], as done by Liu

[4] There is a significant difference between the valve's bend-pass, which is 100[Hz] (according

and Bobrow [2], the position is directly determined by the input to the valve. Hence, $\dot{m}_{choked}$ is a function of the input u,

$$\dot{m}_{choked} = \dot{m}_{choked}(u) \ ,$$

and therefore f_1 must also be a function of u.

- The square root of temperatures, $\sqrt{\frac{T_0}{T_1}}$: T_0 is the ambient temperature, which is constant. T_1 is the supply (or upstream pressure), which can also be considered as constant. The small changes that were spotted occurred only between test sessions. Furthermore, temperature measurements during the valve experiment showed that the differences between T_0 and T_1 were always smaller then 40[K]. Since those temperatures are taken in their absolute scale, we realize that $0.94 < \sqrt{T_0/T_1} \leq 1$. We conclude that the square root of temperature influence over f_1 is negligible, thus, we assume $\sqrt{T_0/T_1} \cong 1$.

We now define a general structure for f_1; according to (D.7), f_1 has the units of a mass flow-rate, therefore we write

$$f_1 = \rho q_{max} \ ,$$

where ρ is the density of air and q_{max} is the maximum volumetric flow-rate at the current conditions. The density, ρ, can be calculated using the ideal gas law (2.6),

$$\rho = \frac{m}{V} = \frac{RT}{P_u} \ ,$$

recalling that m is the air mass, V is the volume of the chamber, P_u is the upstream air pressure, R is the specific gas constant, and T is the air temperature. In order to calculate ρ, we only need to measure P_u. Since ρ is a function of P_u, and f_1 was defined as a function of u, we conclude that q must

to the manufacturer), and the actuator response, which is about 1[Hz]. Therefore, we neglect spool acceleration and velocity and assume immediate response.

also be a function of u. The general form of f_1 is then

$$f_1(P_u, u) = \rho(P_u)\, q_{max}(u). \tag{D.9}$$

To summarize, we see that in order to identify f_1, we only need to determine the dependency of q_{max} on u, as described in detail in section D.5.

D.4.2. f_2 - Flow as a Function of the Pressure Ratio

Examining the engineering approximation model (D.7), we see that the f_2 is a component that is designated to replace the flow function, which is the expression that depends on the pressure ratio, P_r. Therefore, f_2 must also be a function of P_r and behave similarly to the flow function. In section D.6 we include a thorough analysis of the influence of P_r on the flow-rate, and introduce an original fitting model of the flow function.

D.5. Identifying the Maximum Volumetric Flow-Rate

We identify the f_1 component by analyzing the valve test results. According to (D.9), we say that

$$f_1(P_u, u) = \rho(P_u)\, q_{max}(u),$$

where $\rho(P_u)$ is the density of air, which is a function of the upstream pressure, P_u, and $q_{max}(u)$ is the maximum volumetric flow-rate measured, which is a function of the valve's input, u. As explained in subsection D.4.1, $\rho(P_u)$ is directly calculated using the real-time measured P_u and the ideal gas law. Thus, we are left to identify only q_{max} as a function of u.

Figure D.6 displays six data sets: The maximum volumetric flow-rate, q_{max}, and five more data sets of volumetric flow-rate, i.e., q as a function of the input u. Some conclusions from the figure:

- All six data sets have similarly shaped characteristics - similar to the

shape of "S".

- A significant moderation of the incline occur around 6[v] in all the data sets.
- Increasing the input beyond 6[v] (i.e. $u > 6$[v]) hardly changes the flow.
- The difference between data sets is a result of changes in the resistances to flow, for example decreasing the resistance to flow leads to an increase in the maximum flow-rate measured[5].

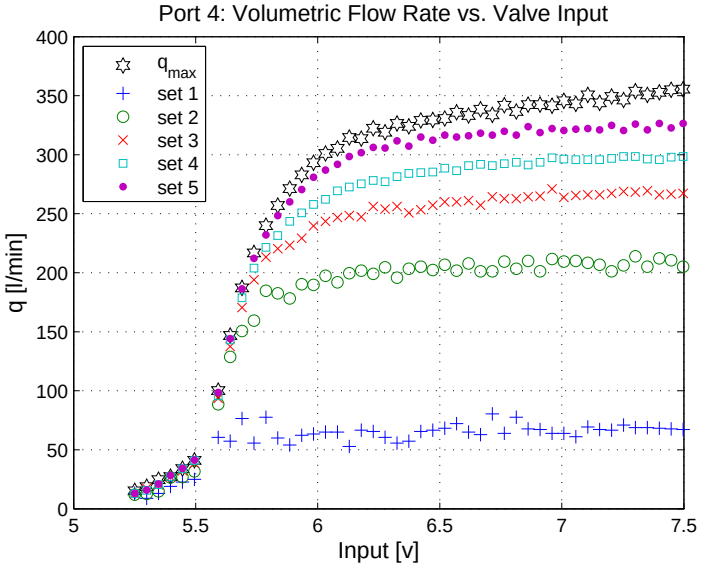

Figure D.6.: Volumetric flow-rate as a function of the valve input

D.5.1. Fit Function for the Maximum Volumetric Flow-Rate

We want to fit an equation that will predict the behavior of the maximum volumetric flow-rate, q_{max}, as a function of the input, u. One possible function that has the shape of "S" is the trigonometric arc-tangent

$$y = \tan^{-1}(x)\,.$$

[5]The variation in the resistance to flow between data sets is achieved by changing the cross section at the valve downstream port. Therefore, less air passes through.

Since it is a symmetric function with respect to the origin, we need to shift the center horizontally and vertically to a desired location; therefore, we consider the hyperbolic version of the tangent function

$$y = \tanh(x) = \frac{e^{2x} - 1}{e^{2x} + 1}. \tag{D.10}$$

The tanh is a symmetric function with respect to the origin, but by introducing some parameters as in (D.11), it can be shifted to any desired location on the xy plane, and we no longer oblige to symmetry. Thus, the empirical fit model is defined by

$$q_{max}(u) = \left(\frac{e^{a_1(u-a_2)} - 1}{e^{a_1 a_3(u-a_4)} + 1} + a_5 \right), \tag{D.11}$$

where a_i for $i = 1...5$ are the fit parameters which are found by optimization methods using the MATLAB curve fitting tool. Figure D.7 shows a comparison between test results and curve fitting of $q_{max}(u)$.

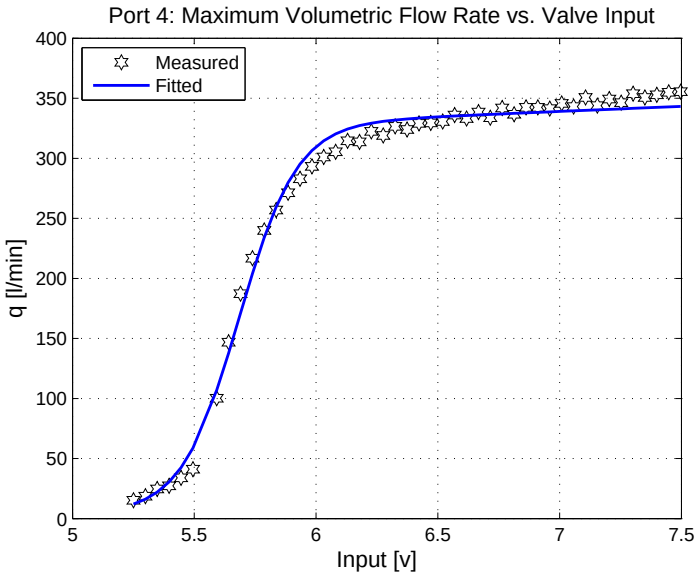

Figure D.7.: Maximum volumetric flow-rate as a function of the valve input - test results and fitted curve

As seen in Figure D.6, the fitted curves pass close to the measured q_{max}.

Fit parameters are shown in Table (D.1) and goodness of fit indexes are: SSE (sum of square error) = 3451, R-square (root square) = 0.994, and RMSE (root mean square error) = 8.96.

Parameter	a_1	a_2	a_3	a_4	a_5
value	42.32	0	0.997	0.1365	5

Table D.1.: Fitted maximum volumetric flow - parameter values

D.6. Identifying the Flow-Rate Function f_2

We continue with the analysis of the valve test results in order to identify the f_2 component. The guideline we follow in the identification process is that f_2 must be a function of the pressure ratio, P_r. Theoretically, we acquire f_2 by manipulating (D.8), such that

$$f_2(P_r) = \frac{\dot{m}(u, P_r)}{f_1(u)}.$$

Since $f_1(u) = \rho q_{max}$ and $m(\dot{u}, P_r) = f_1(u) f_2(P_r)$, we reach the conclusion that $f_2(P_r)$ is a normalized function of the flow-rate. Practically, to identify f_2 we use the same data, shown in Figure D.5, to calculate

$$f_2 = \frac{q}{q_{max}}.$$

Figure D.8 displays seven data sets of f_2 plotted as a function of P_r and the corresponding fit according to (D.13). As can be seen, the extinguishing behavior remains similar to the original data sets, but the maximum magnitude is normalized to unit, which means that f_2 does not change the size of the flow, just like the flow function of the analytic model (see section D.2). The mathematical model of the fitted flow function is then

$$f_2(P_r) = 1 - P_r^a\,, \tag{D.12}$$

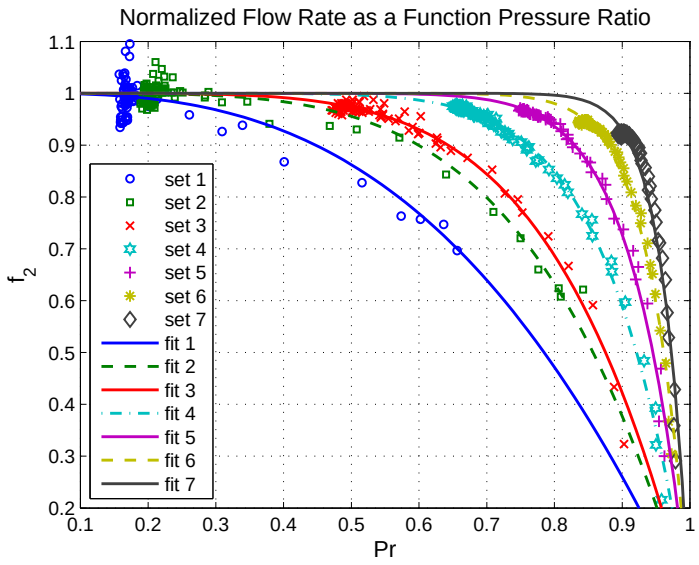

Figure D.8.: Normalized flow-rate and the fitted curves displayed as a function of the pressure ratio for various constant inputs

where a is an exponential parameter which has a different value for each data set. The values of a and the corresponding goodness of fit indexes are summarized in Table D.2.

Set	a	SSE	R-square	RMSE
1	2.86	86.7	0.697	0.998
2	4.49	56.8	0.951	0.808
3	5.21	1095	0.982	3.548
4	8.45	1434	0.991	4.06
5	12.35	3076	0.984	5.946
6	17.63	5020	0.977	7.597
7	25.19	11285	0.950	11.39

Table D.2.: The fit results - parameter values and goodness of fit index

D.6.1. The Exponent Dependency on the Valve's Input

Examining f_2 analysis results in Figure D.8 and in Table D.2, we recognize matching trends of the exponent a and the input u. Thus, we characterize this behavior by using a second order polynomial to relate between a and the

input u. That is, we want to fit a to the equation

$$a(u) = b_1 u + b_2 ,$$

where b_1 and b_2 are the fitting parameters. The results, as seen in Figure D.9, show a good correlation for $b_1 = 11.66$ and $b_2 = -2.99$. The fitting indexes are: SSE $= 24.98$, R-square $= 0.991$, and RMSE $= 0.754$.

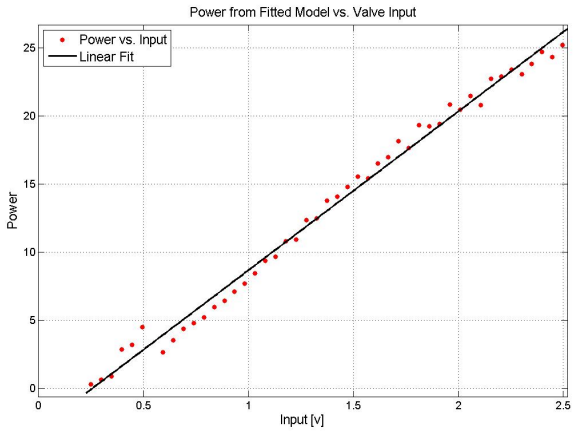

Figure D.9.: Fitted power exponent as a function of input

Finally, we can write the fitted flow-rate function

$$f_2(u, P_r) = 1 - P_r^{(b_1 u + b_2)}. \tag{D.13}$$

To conclude this section, we notice that there is an obvious relation between the identified f_2 function and the valve's input, u. Furthermore, the fitted f_2 has an advantage over the analytical piecewise flow function (see (D.3)), since it holds for the whole range of P_r, i.e., for $0 < P_r < 1$. This advantage is significant for implementation in real time computation application and in simulation.

D.7. The Volumetric Flow-Rate 3D Model

The final step deriving the volumetric flow-rate model is the synthesis of the two models - the maximum volumetric flow-rate, $q_{max}(u)$, and the flow function $f_2(u, P_r)$ into a three dimensional model. The general form of the three dimensional model is then

$$q(u, P_r) = q_{max}(u) f_2(u, P_r),$$

where $q_{max}(u)$ is the identified maximum volumetric flow-rate model given by (D.11) and $f_2(u, P_r)$ is identified flow function given by (D.13). Substituting the complete expressions, we have the explicit volumetric flow-rate model

$$q(u, P_r) = \left(\frac{e^{a_1(u-a_2)} - 1}{e^{a_1 a_3 (u-a_4)} + 1} + a_5 \right) \left(1 - P_r^{(b_1 u + b_2)}\right),$$

where a_i for $i = 1...5$ and b_j for $j = 1, 2$ are the fit parameters that need to be identified specifically for each of the four ports of the valve. In this thesis we demonstrate the identification results only for port 4, as shown in Figure D.10. The surface represents the fitted model and the black dots are the experiment measurements. The fitting indexes are SSE = 51,8170, R-square = 0.988, and RMSE = 11.26.

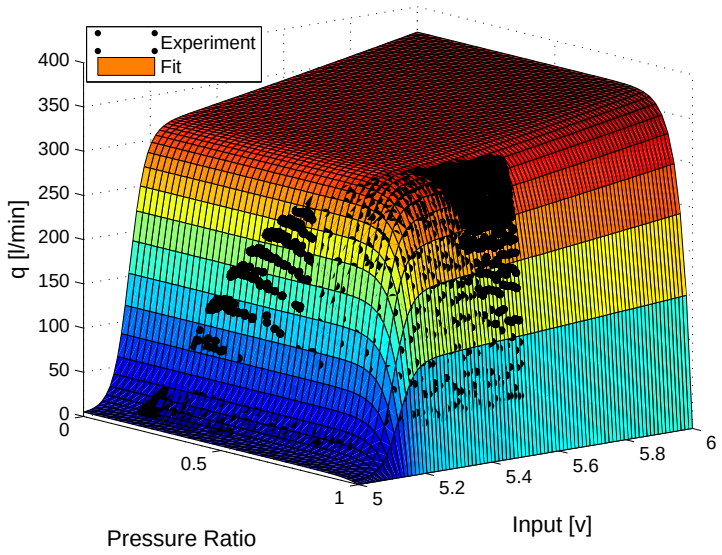

Figure D.10.: Volumetric flow-rate as a function of the input and the pressure ratio

Conclusions

- A very precise model of the volumetric flow-rate was achieved using system identification and analytical model structure.
- The identified model is smooth for the whole range of P_r, which is a major advantage over the piecewise analytical model.
- The identified model, in contrast to the analytical model, reflects the influence of the input u, which makes it more complete.
- Despite the lack of a specific manufacturer's official information on the flow characteristics, the effect of the valve input is modeled and merged into the complete volumetric flow-rate model.

Bibliography

[1] P. Beater, Pneumatic Drives, Springer Berlin Heidelberg, 2007.

[2] S. Liu, J. E. Bobrow, An analysis of a pneumatic servo system and its application to a computer-controlled robot, Journal of Dynamic Systems, Measurement, and Control 110 (1988) 228–235.

[3] J. L. Shearer, Continuous control of motion with compressed air, Ph.D. thesis, Massachusetts Institute of Technology (1954).

[4] E. Richer, Y. Hurmuzlu, A high performance pneumatic force actuator system: Part i-nonlinear mathematical model, Journal of Dynamic Systems, Measurement, and Control 122 (2000) 416.

[5] D. Jeltsema, J. Scherpen, Multidomain modeling of nonlinear networks and systems, Control Systems, IEEE 29 (2009) 28–59.

[6] J. S. H. Goldstein, C. Poole, Classical Mechanics, Addison-Wesley, 2002.

[7] Y. Kawakami, J. Akao, S. Kawai, T. Machiyama, Some considerations on the dynamic characteristics of pneumatic cylinders, Journal of Fluid Control 19 (1988) 22–36.

[8] H. K. Khalil, Nonlinear Systems; 3rd ed., Prentice-Hall, 2002.

[9] J. Wang, J. Pu, P. Moore, A practical control strategy for servo-pneumatic actuator systems, Control Engineering Practice 7 (1999) 1483–1488.

[10] J.-Y. Lai, C.-H. Menq, R. Singh, Accurate position control of a pneumatic actuator, in: American Control Conference, 1989, IEEE, 1989, pp. 1497–1502.

[11] E. Richer, Y. Hurmuzlu, A high performance pneumatic force actuator system: Part ii-nonlinear controller design, Journal of Dynamic Systems, Measurement, and Control 122 (2000) 426.

[12] Z. Rao, G. Bone, Modeling and control of a miniature servo pneumatic actuator, in: Robotics and Automation, 2006. ICRA 2006. Proceedings 2006 IEEE International Conference, IEEE, 2006, pp. 1806–1811.

[13] J. Wang, Backstepping, Wikipedia.

[14] F. Verhulst, Nonlinear Differential Equations and Dynamical Systems, Springer Verlag, 1996.

[15] FESTO - Proportional Directional Control Valves MPYE.

[16] Iso 6358: Pneumatic fluid power - components using compressible fluids - determination of flow-rate characteristics (10 1989).

[17] O. Olaby, X. Brun, S. Sesmat, T. Redarce, E. Bideaux, B. LAI, A. de Lyon, Characterization and modeling of a proportional valve for control synthesis, Proceedings of the 6th JFPS International 3 (2005) 1.

תקציר

מערכות הינע פניאומטיות נתפשו במשך שנים רבות כנושא שנוי במחלוקת בתחומי האוטומציה והבקרה. יתרונותיהן הרבים, כגון יחס גבוה של משקל לכוח, ניקיון, עלות נמוכה, אמינות ופשטות, תרמו להפצתן בתעשייה ובמיוחד בתחומי האוטומציה והשינוע. מצד השני, השימוש בזורם דחיס (בדרך כלל אוויר) מקשה על היכולת לחזות באופן מדוייק את ההתנהגות הדינמית של המערכת. חסרון זה הגביל, לאורך השנים, את מאמצי פיתוח הבקרה ליישומי הינע בחוג פתוח בהם לא נדרש דיוק.

בתזה זו אנו מפתחים בקרת מיקום מדוייקת למערכת הינע פניאומטית. שימוש בשיטת ה-backstepping מאפשרת עקיבה מדוייקת אחר אות יחוס משתנה של מיקום, כאשר על המנוע הפניאומטי (pneumatic actuator) פועלת הפרעה של כוח חיצוני משתנה בזמן. כדי להוכיח את ישימות השיטה, הטמענו את הבקר על מערכת ניסוי. תוצאות הניסוי המדווחות מציגות ביצועים מצויינים של מעקב אחר אותות ייחוס בצורת גל סינוס וגל ריבועי. במהלך הניסויים על המנוע הפניאומטי פעל כוח חיצוני בעוצמה המשתנה ברציפות בין 250[N] ל- 1050[N].

כשלב מקדים לפיתוח הבקרה, אנו מציגים גישה חדשה לניתוח ולמידול של מערכת ההינע הפניאומטית. במקום להשתמש בגישה הרווחת של ניתוח הכוחות הפועלים במנוע הפניאומטי, אנו מפתחים את המודל הדינמי על בסיס שיקולי אנרגיה. תחילה אנו מציגים את האנרגיה הקינטית והפוטנציאלית, באמצעותם מתקבל את הלגרנג'יאן (Lagrangian) של המנוע הפניאומטי, ולבסוף אנו גוזרים ממנו את משוואות התנועה של המערכת.

אל עף שלצרכי פיתוח הבקרה השתמשנו במודל מפושט של הספיקה המסית דרך השסתום, הוספנו נספח ובו שיטה מקורית ומקיפה למידול מדוייק שלה. בשיטה זו אנו מתאימים מודל תלת מימדי של הספיקה המסית כתלות במתח ובלחצים באמצעות ניסוי. על פי תוצאות הניסוי/בבחינת המודל נמצא כי קיים מתאם גבוה בינו לבין הספיקה בפועל. כמו כן, שיטה זו ניתנת ליישום על שסתומים נוספים.

אוניברסיטת בן-גוריון בנגב
הפקולטה למדעי הנדסה
המחלקה להנדסת מכונות

בקרת מיקום מדויקת למערכת הינע פניאומטית

חיבור זה מהווה חלק מהדרישות לקבלת תואר "מגיסטר" בהנדסה

מאת:

אדי זיסר

מנחים:

ד"ר אמיר שפירא

ד"ר רזיאל רימר

חתימת מחבר: _____ תאריך: _____

חתימת מנחה: _____ תאריך: _____

חתימת מנחה: _____ תאריך: _____

אישור יו"ר ועדת מוסמכים מחלקתית: _____ תאריך: _____

אדר תשע"ג *פברואר 2013*

אוניברסיטת בן-גוריון בנגב
הפקולטה למדעי הנדסה
המחלקה להנדסת מכונות

בקרת מיקום מדויקת למערכת הינע פניאומטית

חיבור זה מהווה חלק מהדרישות לקבלת תואר "מגיסטר" בהנדסה

מאת:
אדי זיסר

אדר תשע"ג *פברואר 2013*